



# Groundwater Project and eBooks: An Evolving Platform for Groundwater Education and Practice

“Knowledge is power. Information is liberating. Education is the premise of progress, in every society, in every family.”

- Kofi Annan, 1997

“Knowledge should be free and the best knowledge is free knowledge.”

- Ying Fan Reinfelder, 2019

**Edited by**

John Cherry, G360 Institute for Groundwater Research, University of Guelph and  
Distinguished Emeritus Professor, University of Waterloo, Canada

10/02/2020

Gmail - Your manuscript has been accepted



Jaime Garfias <jgarfiass@gmail.com>

---

## Your manuscript has been accepted

1 mensaje

---

**Amanda Sills** <amanda.sills@g360group.org>  
Para: Jaime Garfias <jgarfiass@gmail.com>

10 de febrero de 2020, 9:03

Dear Dr. Garfias,

We are pleased to inform you that your chapter, "Case study: Assessment of groundwater exploitation and land subsidence development in the Toluca aquifer system, Mexico", has been accepted for publication in the Ebook: An Evolving Platform for Groundwater Education and Practice. You will receive an-email in due course regarding the production process.

With best regards,

**Amanda Sills**, MSc, P.Geo.

**Ebook Coordinator**

[G<sup>360</sup> Institute for Groundwater Research](#)

College of Engineering & Physical Sciences | University of Guelph

50 Stone Rd E Guelph, ON, N1G 2W1

(519) 824-4120 ext. 53940 | [amanda.sills@g360group.org](mailto:amanda.sills@g360group.org)

**Table 3: eBook Contributors Associated With 148 Organizations - September 13, 2019**

Europe	North America	
Aarhus University	AECL	Shell Global Solutions
Beicip-Franlab	AECOM	Southwest Research Center
British Geologic Society	Air Force Institute of Technology	Stanford
Delft University of Technology	American Petroleum Institute	Syracuse University
ETH Zurich	ARCADIS	S.S.Papadopolous
Federal Inst. Geosci. & Ntrl Resources	Atomic Energy of Canada	Temple University
Geolog./ Geophysical Inst. of Hungary	Arizona State University	Tetrattech
Geological Survey of Denmark and Greenland	Beatty and Associates Consulting	TRC Consulting
Karlsruhe Institute of Technology	BP	The University of New Mexico
University College London	Baker Law	The Water Institute U of Waterloo
Universite de Recherche INRS	Brown University	U.S. Geological Survey
University of Basilicata	Burns & McDonnell	UC Santa Cruz
University of Belgrade	Carleton University	Universite de Recherche INRS
University of Bologna	Chevron	University of Alberta
University of Lausanne	Colorado School of Mines	University of British Columbia
University of Leeds	Colorado State University	University of Buffalo
University of Liege	Columbia University	University of Calgary
University of Montpellier	Dalhousie University	University of California Davis
University of Oslo	Dickinson College	University of Guelph
University of Padova	Dillon Consulting	University of Houston
Sapienza University of Rome	Dordt University	University of Iowa
Sorbonne University	Environment Canada	University of Kansas
University of Strasbourg	EPA	University of Laval
University of Strathclyde	Exxon	University of Liege
Wageningen University	Geofirma Engineering Ltd.	University of Minnesota
World Health Organization	Geologic Survey of Canada	University of Montana
Asia	Georgia Tech	University of Nebraska
China University of Geosciences	Golder	University of New Brunswick
South China University of Sc. and Tech.	Geochimica	University of Nevada
University of Hong Kong	Haley Aldrich Consulting	University of Ottawa
South Africa	Hess Corp.	University of Quebec
Groundwater Africa	Hydrodynamics Group	University of Saskatchewan
Metago Water Geosciences	Integrated Sustainability Cnsltg	University of South Florida
Parsons and Assoc. Groundwater Consultants	King's College	University of Tennessee
Sinopec Research Institute	Mercer University	University of Texas
University of Free State	McGill University	University of Toronto
University of Pretoria	Michigan State University	University of Utah
University of Western Cape	NGWA	University of Washington
South and Central America	Natural Resources Canada	University of Waterloo
Autonomous University of the State of Mexico	New Mexico Tech	University of Quebec
Brazilian Geologic Survey	Orange County Water District	University of Wisconsin-Madison
City of Sao Paulo	Oregon State University	US Army Corps of Engineers
Federal University of Rio De Janeiro	Pacific Northwest Natl. Laboratory	USGS
Hidroplan Sustainable Water Institute	Princeton University	US Federal Institute Geoscience & Natural Resources
University of Sao Paulo	Partners in Hope	USGS Water Res. Mission Area
Vectfor	QED Environmental System	Vista Clara
Australia	Queen's University	Western University
Flinders University	Rutgers	Wilfrid Laurier University
CSIRO	Sacramento State University	World Bank

Domain Lead Kamini Singha

1. Overview: Role of geophysics in hydrogeologic problems: Kamini Singha, Frederick Day-Lewis
2. Electrical Resistivity: Frederick Day-Lewis, Kamini Singha, Tim Johnson
3. Induced Polarization:
4. Ground-penetrating Radar: Colby Steelman
5. Electromagnetic Induction: Anders Vest Christiansen
6. Self Potential: Damien Jougnot, Emily Voytek
7. NMR: Elliot Grunewald, Kristina Keating
8. Seismic: Jordan Hayes, Brady Flinchum
9. Fiber Optics: Scott Tyler, Nick van de Giesen, John Selker
10. Wireline Logging: John Williams
11. Airborne Methods: Burke Minsley
12. Tools for Fractured Rock
13. Rock Physics: Fred Nguyen
14. Joint Inversion: Erasmus Oware

### **38. IMPORTANT AQUIFER SYSTEMS AROUND THE WORLD**

*Chapters of the Domain:*

1. High Plains Aquifer: USA
2. Edwards Aquifer: USA - Jack Sharp and Ron Green
3. Dakota Aquifer: USA
4. Milk River Aquifer: USA-Canada
5. California Central Valley Aquifer System: USA
6. Ogallala Aquifer: USA
7. Guarani Aquifer System: Brazil, Argentina, Paraguay, Uruguay - Roberto Kircheim
8. Permo-Triassic Aquifer: UK
9. the Chalk aquifer UK
10. Mexico Exemplary Example: Toluca Aquifer - Jaime Garfias
11. Mexico Valley Aquifer

### **39. COUNTRY BY COUNTRY OVERVIEWS OF HYDROGEOLOGY, GROUNDWATER USE AND PROBLEMS**

### **40. DRILLING AND CORING METHODS**

*Chapters of the Domain:*

1. Manual Well Drilling
2. Mechanized Well Drilling
3. Drilling Groundwater Monitoring Wells
4. Overburden Coring

### **41. STREAM, LAKE AND OCEAN MEASUREMENTS**

*Chapters of the Domain:*

1. Stream Assessment and Gauging: Kamini Singha

# Groundwater Project and eBooks: An Evolving Platform for Groundwater Education and Practice

## Case study: Assessment of groundwater exploitation and land subsidence development in the Toluca aquifer system, Mexico

Jaime Garfias<sup>1</sup>, Richard Martel<sup>2</sup>, Angus Calderhead<sup>2</sup>

<sup>(1)</sup> Inter-American Institute of Technology and Water Sciences (IITCA). Autonomous University of the State of Mexico, Toluca, Mexico, C.P. 50130, Email: [jgarfiass@gmail.com](mailto:jgarfiass@gmail.com)

<sup>(2)</sup> Institut National de la Recherche Scientifique (INRS-Été), Québec, QC G1K 9A9 Canada, Email: [richard.martel@ete.inrs.ca](mailto:richard.martel@ete.inrs.ca), [aicalderhead@gmail.com](mailto:aicalderhead@gmail.com)

### Abstract

Rapid population growth in the Toluca region place increasing demands on the availability of water resources. The increased groundwater pumping has resulted in a systematic decline of the water table, the disappearance of artesian springs and wetlands, as well as subsidence within the basin. There is an imminent need to conduct groundwater studies and to implement protection strategies to ensure the long-term sustainability of clean water supplies in the region. To address these concerns, a multidisciplinary approach is presented here for quantifying land subsidence in a heavily pumped aquifer system with complex stratigraphy. The methodology consists in incorporating Terzaghi's 1D instantaneous compaction principle into a 3D groundwater flow model that is then applied and calibrated to reproduce observed hydraulic heads and compaction for the Toluca aquifer system, Mexico. Differential Interferometric Synthetic Aperture Radar (D-InSAR), a generated 3D-geological model, extensometers, monitoring wells, and available literature are used to constrain the model. The results indicate that shrinking water availability is due mainly to anthropogenic effects and that the current pumping rates are not sustainable. The D-InSAR measured subsidence, extensometers, and numerical simulations of subsidence agree relatively well. Simulations show that since regional subsidence began in the mid 1960s there has been up to 2 m of subsidence in the industrial corridor, where heavy pumping and thick clay layers are found. This study shows that an approach using various sources of data is useful in estimating and constraining the vertical component of the inelastic skeletal specific storage. The declining groundwater levels in the Toluca aquifer are a challenge for Resource managers and stakeholders to minimize the hazards while maximizing the beneficial use of the resources.

**Key words:** HydroGeoSphere model, InSAR, Land subsidence, Overexploitation, Toluca.

### 1. Introduction

Aquifer-system compaction and land subsidence due to water withdrawal is a growing hazard affecting many urban areas in the world and constituting a major threat to the sustainable development of nations (Tessitore et al., 2016). This phenomenon is usually associated with different simultaneous processes: ineffective aquifer management, increases in population and the related increment of the groundwater exploitation. Furthermore, the experience of recent years

confirms a lack of detailed analysis of groundwater recharge and, in most cases, an incomplete survey of groundwater extraction (Calderhead et al., 2011). Thus, groundwater flow and compaction numerical models are useful tools to analyze land subsidence and they represent the best known method available for predicting subsidence. Although other approaches, such as analytical models or extrapolation, are less data intensive, they often lack spatial detail.

Since the emergence of numerical groundwater flow models in the 1970s, there have been several studies where compaction has been coupled to groundwater flow. Since Gambolati and Helm's pioneering work in the early 1970s (Gambolati, 1972; Helm, 1975), most models have represented compaction by incorporating Terzaghi's 1D compaction principle into the groundwater flow equation, which is then solved by finite differences (Helm, 1975; Hoffmann et al. (2003b); Leake and Prudic (1991); Lui and Helm (2008). Biot's 3D derivation (Biot, 1941) is sometimes used (Burkey and Helm, 1999; Burkey, 2001, 2005; Hsieh, 1996; Lewis and Schrefler, 1978; Safai and Pinder, 1979) and the resulting equations are usually with the finite element methods. Over the years, various compaction aspects have also been included in models such as stress dependent storage properties (Helm, 1976); dependence of compaction on hydraulic conductivity (Rudolph and Frind, 1991), time delays (Hoffmann et al., 2003a; Hoffmann et al., 2003b), and effects of moving water tables (Leake and Galloway, 2007; Liu and Helm, 2008).

Nevertheless, data scarcity remains a major limitation to model applications and to the reliability of their predictions. Except for a few heavily studied major urban centers such as Mexico City, Bologna, Texas; Arizona, Shanghai and Murcia (Osmanoglu et al., 2011; Bonsignore et al., 2010; Chaussard et al. (2014); ADWR, 2011; Ye et al., 2012; Tomás et al. 2009; Tessitore et al., 2016), and a few non-urban centers such as Antelope Valley, California, and South-Central Arizona (Hoffmann and Zepker, 2003c; Conway, 2016), subsidence data is often incomplete mostly because extensometer installations needed to measure land subsidence have high costs. Even where extensometers exist, there is often a lack of long term monitoring data needed for model calibration.

Synthetic Aperture Radar Interferometry (InSAR) is based on the difference between the phase from two processed SAR complex images acquired from two different positions. Differential InSAR (D-InSAR) removes the topography component of the measured phase by using a Digital Elevation Model (DEM). In ideal conditions such as dry climates with little vegetation, spaceborne InSAR has the ability to monitor land movement at the regional scale with sub-centimeter vertical precision (Hanssen, 2001). As it is known, recent advances and applications in interferometry (e.g., Persistent Scatterers Interferometry (PSI) and Small BAseline Subset (SBAS)) increase the confidence in the results by using a large time series of SAR images (Ferretti et al., 2000, 2001; Berardino et al., 2002). These new techniques would have been the preferred method for determining total compaction (or subsidence) over D-InSAR because more confidence is given to results (Gambolati and Teatini, 2019). However, due to restrictions in obtaining capable software, and due to ease of use, D-InSAR was the selected method for measuring compaction. D-InSAR data can be less precise due to phase noise from decorrelation in vegetated areas and atmospheric effects (Zebker et al., 1997) and thus has to be handled with care for deterministic numerical models (Hanssen, 2001). Nonetheless, this technology provides excellent data to calibrate subsidence models even where very little compaction field data is available.

Due to little interaction between remote sensing communities and hydrogeologists, only a handful of subsidence studies have combined groundwater flow and compaction numerical models with remote sensing techniques and field data (Galloway and Hoffmann, 2007). Amelung et al. (1999) has contrasted clay thickness maps with D-InSAR subsidence patterns. Galloway et al. (1998), Hoffmann et al. (2003a) have presented finite difference delayed-compaction models constrained by D-InSAR results and field data for several subsiding locations in Nevada and California. In spite of all this, there is a need to further explore the use of InSAR data to calibrate numerical models that simulate land subsidence.

This chapter presents an integrated and systematic summary of the new approach applied in the Toluca aquifer system, which includes water budget estimation and Terzaghi's 1D instantaneous compaction principle into the HydroGeosphere (HGS) finite element groundwater flow model (Therrien et al., 2009). The incorporation of compaction in the flow model is verified and the model is demonstrated by reproducing land subsidence caused by pumping in the Toluca Valley, Mexico. Simulations are constrained by remote sensing and field data for the complex aquifer system of the Toluca Valley. Hoffmann et al. (2003a) demonstrates that D-InSAR is useful for deriving the total inelastic skeletal storage coefficient  $S'_{sk}$  of an aquifer. Their approach, however, does not consider the vertical variability of  $S'_{sk}$ . In complex aquifer systems, such as in the Toluca Valley, Mexico, with vertically variable material properties, assigning inelastic skeletal storage coefficient for individual clay layers becomes more problematic and requires other sources of data. This work extends the general approach used by Galloway et al. (1998), Amelung et al. (1999), Hoffmann et al. (2003a) by using D-InSAR subsidence estimates and further constrains the groundwater flow-compaction model with a 3D geologic model to derive  $S'_{sk}$  for individual clay layers. Additionally, multiple remote sensors are used over a 5-year period, thus increasing confidence in D-InSAR estimates. The multidisciplinary approach not only demonstrates the utility of various investigative approaches in evaluating the aquifer-system compaction of the overexploited aquifer but also provides insight into some of the factors that control the impacts of groundwater extraction on the aquifer system in general.

## 2. Description of the study area

The Upper Lerma River Valley is situated in the Trans-Mexican Volcanic Belt (*TMVB*), a chain of mountains of Oligocene to recent age, which crosses Mexico from the Pacific Ocean to the Gulf of Mexico (Nelson and Sanchez-Rubio 1986). The Upper Lerma River Basin is subdivided into two basins, the Toluca Valley Basin to the south and the Ixtlahuaca Basin to the north (Fig. 1). The valley, with an elevation of about 2,600 *masl*, covers an area of about 2,100 km<sup>2</sup> (Gárfias et al., 2008) and is surrounded by mountain ranges to the east, south and west (CONAGUA, 2002). Along the southern and western boundaries of the basin, lie the Nevado de Toluca and Cerro de Tenango volcanoes, which divide the Toluca Basin and the Balsas-Mezcala Basin (Gobierno del Estado de México 1997; Eteisa 1997) (Fig. 1). The Toluca Valley's geographic position in the center of the country and proximity to Mexico City, as well as its rapidly developing infrastructure, have allowed the city to grow into a major industrial zone for the country.

The rainy season generally occurs during the months of April through October. Annually, the basin valley receives an average of 695 mm of precipitation (Lesser and Asociados, 1992), whereas the higher altitudes receive larger amounts of rain, in the range of 1,200 *mm/year* (Gobierno del Estado de México, 1997). During the winter months, precipitation often falls as snow on the Nevado de Toluca volcano (Eteisa, 1997). Annual precipitation cycles and amounts in the basin have been relatively constant since the first year of available data in 1942 (Lesser and Asociados, 1992).

According to the 2015 population estimates by region [CONAPO, 2015], the metropolitan area of Toluca, including 15 neighboring municipalities, is the fifth most populous metropolitan area in Mexico and the largest within the State of México. The total population of the Toluca Valley in 2015 was just over 2.2 million people (CONAPO, 2015). From 1960 to 2015, the population of the valley has doubled approximately every 20 years (INEGI, 1960; CONAPO, 2015). The following subsections describe the available data and associated pre-processing: Geological information used to generate a 3D geological model.

## 2.1 Hydrogeology and Groundwater exploitation

The regional groundwater flow within the Toluca Basin, for the most part, is controlled by topography, where the primary recharge to the aquifers is in the mountains. Outcrops of fractured andesitic and basaltic rocks and pyroclastic material in the Nevado de Toluca and the Cruces mountains facilitate the direct infiltration of precipitation to the aquifer, which then flows horizontally towards the centre of the valley (Eteisa, 1997; Grupo Herra, 1992). Groundwater flows preferentially in the aquifers through more permeable layers and channels in the fractured materials (Eteisa, 1995). Whereas historically, groundwater discharged in springs along the edges of the valley, and into the Lerma River system and the chain of lakes in the valley, extensive extraction from pumping wells throughout the valley have modified the historical groundwater flow patterns (Eteisa, 1995; Grupo Herra, 1992). Since the early 1950s, the regional groundwater flow field has been significantly affected by local groundwater extraction with the largest impacts associated with the Lerma system wells (Figs. 1 and 2), which has drawn flow towards the eastern flanks of the basin (CONAGUA, 2002; Eteisa, 1997).

Historically, in the Toluca Valley, groundwater levels were either at depths close to the surface or emerged above the land surface in artesian conditions (Lesser and Asociados, 1992). Currently, there is a significant decrease in the water level within the basin, primarily due to groundwater pumping, and the decrease is increasing with time (Calderhead et al., 2010). There are more than 935 pumping wells in the Toluca Valley (IMTA, 2003). Groundwater exports occur in the form of the Lerma system wells, a groundwater pumping system operated by Mexico City and consisting of 230 pumping wells located along the upper section of the Lerma River (Fig. 2). The system has been in operation since the late 1960s and captures a large portion of the recharge water entering from the Sierra Las Cruces which is then exported to Mexico City at approximately 6.0 m<sup>3</sup>/s (Hancox et al., 2010; Rudolph et al., 2006). Increasing local demand for water has also added stresses on the aquifer system.

## 2.2 Geological setting

Volcanic andesitic rock from a Miocene-age buried volcano in the center of the valley forms the basement in the basin (Fig. 3). The bedrock forms a bowl in the center of the valley, reaching depths greater than 600 m and cropping out to the surface at the edges of the valley. The andesitic volcano formation of the Nevado de Toluca core is located to the south-west. The bedrock is overlain by a confining layer of pure lacustrine clays and by the Chalma formation aquifer, composed of a mixture of sand, gravel and clay. The Tarango formation aquifer, deposited after the Chalma formation, extends from the flanks of the Sierra Las Cruces Mountains in the East across the basin floor to the foot of the Nevado of Toluca volcano. This formation is a heterogeneous mixture of volcanoclastic materials (Lesser and Asociados, 1992). The basaltic and ash flows of the Chichinautzin formation were deposited in the eastern portion of the Toluca Valley and act as an aquifer. In the upper middle portion of the valley, where most of the groundwater pumping occurs, complex interlayering of lacustrine clay (aquitar) and alluvium deposits (aquifer) are found. The industrial corridor, adjacent to the Lerma River (Figs. 2 and 3), is located on what used to be a flood plain. Occasionally, during heavy rainfall, parts of the industrial corridor become a flood plain, yielding more compressible sediment. The complex sequence of layers in this area is shown schematically in Fig. 4.

Clay materials are known to be significantly more compressible than other common materials such as sand, gravel, or consolidated rock. It is thus important to delineate the clay layer boundaries for a proper representation of a compaction model. Amelung et al. (1999) describe the correlation between InSAR derived subsidence and aggregate clay thickness (the sum of clay layer thicknesses at a given xy-location). There are several types of clays in the Toluca valley, varying from very low compressibility ( $\bar{\alpha} = 2 \times 10^{-8} \text{ Pa}^{-1}$ ) to moderately high compressibility ( $\bar{\alpha} = 3 \times 10^{-6} \text{ Pa}^{-1}$ ). From the geological model presented in the previous section, four distinct clay layers are delineated



in addition to the computed aggregate clay thickness. Based on these data, Fig. 5 presents the two major (Fig. 5a and 5b), and aggregate (Fig. 5c) clay layers.

### 3. Methodology

The methodology used for this study includes (1) improving the groundwater budget model in order to determine the future deficit and water availability; (2) integrating compaction to the groundwater flow model and validation; and (3) setting up and calibrating the model for the Toluca Valley and description of the SAR image data employed to estimate surface displacements related to aquifer-system deformation.

#### 3.1 Water budget and hydraulic head distribution

The groundwater budget in the Toluca Valley has been evaluated by SRH (1970); Lesser and Asociados (1992); Ariel Consultores (1996); CONAGUA (2002); and GTZ-CNA (2004). These studies, however, lack a detailed analysis of the groundwater balance and present, in many cases, an incomplete survey of inputs (recharge) and outputs (pumping and natural discharge). To evaluate recharge, the above studies did not take into account several parameters and in several cases results were averaged over large territories. This study includes spatially variable recharge determined from the historical climate data, the climate change predictions, and the multiple parameters used in the Hydrologic Evaluation of Landfill Performance (HELP3) model to estimate the past, current and future recharge distributions. In the present study, the total recharge ( $Q_{on}$ ), the total discharge ( $Q_{off}$ ), and the rate of change in storage ( $\partial V/\partial t$ ) are defined with units [ $L^3/T$ ] (for the purposes of this work, the units are assigned  $Mm^3/year$  or millions of cubic meters per year) and represented by the following relation:

$$Q_{on} - Q_{off} \pm \frac{\partial V}{\partial t} = 0. \quad (1)$$

The sign of  $\partial V/\partial t$  is positive if there is a deficit and negative if there is a surplus. Using recharge, discharge, and pumping terms, Eq. 1 becomes:

$$R - (D + P) \pm \frac{\partial V}{\partial t} = 0, \quad (2)$$

where  $R$  is the recharge rate, generally assumed to come from precipitation,  $D$  is the discharge rate ( $Mm^3/year$ ) or water that is not captured by pumping such as discharge to streams and lakes, evaporation, evapotranspiration, and  $P$  is the net rate of extraction from pumping wells ( $Mm^3/year$ ). Each parameter of Eq. 2 is examined closely for the case of the Toluca Valley.

Considering the hydrologic behaviour of the Toluca Valley and the HELP3 model components, equation 2 can be rewritten as:

$$(R_0 + R_{art}) - (GW_{flow} + S_p + P) \pm \frac{\partial V}{\partial t} = 0, \quad (3)$$

where the recharge ( $R$ ) from Eq. 2 is the sum of the natural recharge ( $R_0$ ) and the artificial Recharge ( $R_{art}$ ). The Discharge rate ( $D$ ) (Eq. 2) is the sum of groundwater flow ( $GW_{flow}$ ) and spring discharges ( $S_p$ ).

With the objective of combining Eq. 3 with the parameters used in HELP3, and considering the hydrologic behaviour of the Toluca Valley, the water budget for the Toluca Valley is described by equation 4:

$$\left( R_0 \begin{pmatrix} R_P, R_T, R_{RL}, R_{rad}, R_{LAT}, R_{GS}, \\ R_{LAI}, R_{ED}, R_{SCS}, R_b, R_\theta, R_{WP}, \\ R_{FC}, R_{k_{sat}}, R_{DD}, R_{SL} \end{pmatrix} + R_{art} \right) - GW_{flow} - S_p - P \pm \frac{\partial V}{\partial t} = 0, \quad (4)$$

For the present study, Eq. 2 was modified to represent the natural recharge ( $R_0$ ) (Eqs. 3 and 4) as a function of the parameters used in HELP3. The overall approach of this study is to use all available data to simulate the groundwater budget of the Toluca Valley. HELP3 simulations provide a spatially variable representation of the historical and climate change predictions of recharge using daily data input values to obtain yearly recharge estimates. Historical and predicted yearly discharges from the aquifer (with average, the best, and the worst case scenarios) are calculated as a function of groundwater pumping, groundwater flow off the basin, change to the discharge rate, and spring discharge. Both the total discharge and recharge are summed with the objective of quantifying the historical and projected groundwater deficit. Recharge values, needed for the flow simulations, are based on meteorological data between 1970 and 1999. An average recharge value is used for the period 2000–2010 (CONAGUA, 2006). For more details concerning the multiple parameters and sources of data used in the HELP3 model, the reader can refer to Calderhead et al. (2012b).

Based on 48 multilevel piezometers operating in the Toluca Valley since 1969, (CONAGUA, 2008) documents drawdown within the valley over a four decade period. Drawdown is induced by over 935 pumping wells with varying pumping rates located throughout the Toluca Valley (Fig. 2). For simplification purposes, 167 representative wells at selected locations are used to represent all pumping occurrences. Based on IMTA (2003) and Calderhead (2009), total pumping is distributed evenly between the 167 representative wells.

The hydraulic head distribution throughout the valley has been in steady decline since the mid 1960s. Intense pumping near the city center has led to the formation of a cone of depression. Predictions into the future see a decrease in the hydraulic head (Ariel and Consultores, 1996; Calderhead, 2009; Lesser and Asociados, 1992).

### 3.2. Groundwater flow and compaction model

The research approach used in this study consists in incorporating Terzaghi's 1D instantaneous compaction principle into the HydroGeosphere (HGS) finite element groundwater flow model (Calderhead et al., 2011). The compaction component is based on Terzaghi's 1D effective stress principle as applied by Hoffmann et al. 2003b(23), Leake and Galloway (2007)(36), Liu and Helm (2008)(39). Calderhead et al. (2011), Galloway and Burkey (2011), Liu and Griffiths (2015) provide additional background on analysis and modeling of land subsidence accompanying deformation of aquifer systems. The new compaction module in HGS was tested by reproducing a simulation performed with MODFLOW-SUB, a widely used and verified model. Sample problem 2 from (Hoffmann et al. 2003b) which simulates the effects of seasonally fluctuating stresses on heads in an aquifer was selected, and set up in both MODFLOW-SUB and HGS. The resulting computed head and compaction was identical for both models, giving confidence that HGS correctly solves the groundwater flow equation with compaction, which is the same equation solved by MODFLOW-SUB (Calderhead et al., 2011). The advantage of using HGS over MODFLOW-SUB for simulating 3D fluid flow and compaction is that HGS uses the control volume finite element method to solve the governing equation, with a finite-element-based mesh to discretize the simulation domain. The finite-element mesh provides more flexibility than the integrated finite element method used in MODFLOW-SUB to represent irregular geometries, such as those found for geological layers in the

Toluca Valley. Simulations were constrained by remote sensing and field data for the complex aquifer system of the Toluca valley.

### **3.3 Subsidence measurements**

Historical geodetic information and accurate field subsidence measurements were not available for the Toluca Valley. The objective of installing the extensometers was to obtain accurate field measurements at point locations. Two R-4 magnetic reed switch probe extensometer systems by Roctest Ltd. (2009) were installed in the industrial corridor (Fig. 6). Boreholes with a 15 cm diameter were bored by a rotary drill and reach depths of 115 and 78 m, respectively, for Extensometer-1 and Extensometer-2. The extensometers (Fig. 6) consist of magnetic targets, surrounding the centre of a 7 cm radius, 6 m long PVC pipe; the 6 m sections of PVC pipe are separated by telescopic joints. The spring anchors attached to the PVC pipe and joined by telescopic joints are lowered to the bottom of the borehole and then released with an external draw wire. Any compaction or swelling below the bottom anchor is not measured by the extensometer.

Once the extensometer is installed, a magnetic probe, lowered down the access pipe, detects the position of the magnet anchors. The probe is suspended by a single graduated tape that incorporates the electrical leads. The tape graduation is used to determine the deformation between magnetic anchor points along the pipe axis. For this study, reading frequencies from the extensometers varied from 1 to 6 months and spanned 2 years beginning in July 2006 and ending in July 2008.

Extensometer-2 is located northeast of Extensometer-1 (Fig. 4). The location was chosen due to noticeable subsidence affecting structures. To ensure all compaction is measured, it would have been preferable to have the bottom of the extensometer reach bedrock. By observing adjacent borehole logs, it is expected that the bedrock is probably located well below 300 m depth. Thus, the cost and technical difficulty prohibited reaching the bedrock. However, it is estimated that most of the compaction due to pumping occurs in the upper 100 m of the groundwater flow system, where the pores lose saturation, compressible materials are newer, and clay content is high.

In addition, InSAR derived subsidence maps were used to estimate and decrease the uncertainty associated with specific storage values. The interferograms and deformation maps are useful for locating compacting regions and quantifying the amount of subsidence. SAR images were obtained from ERS-1, ENVISAT ASAR, and RADARSAT-1 between 1996 and 2008. Calderhead et al. (2010) present the complete D-InSAR results for the Toluca Valley. Based on the above analysis, Fig. 10b shows an example of an interferogram of two images taken 70 days apart in late 2007 and early 2008.

### **3.4. Model setup and calibration**

#### **3.4.1. Model setup of the 3D geology**

A common problem in generating a representative 3D geological model is a lack of data. The best way to improve the 3D model is by using a large number of borehole logs. Fortunately, a significant number of logs are available for the Toluca Valley. To deal with the complex stratigraphy of the Toluca Valley, a processing chain uses borehole logs for generating a representative regional 3D geologic model. A total of 211 geologic well logs (Fig. 7a: 151 Lerma pumping wells, 48 multi-level piezometers, and 12 additional wells) from the Toluca Valley basin were used to create the 3D geologic model domain. The 22 geologic types ranging from clays and fine sands to coarse gravel and volcanic fractured rock were simplified into 10 material types. Based on the well data and existing cross sections, the GMS 6.5 software uses a sequence of algorithms (GMS, 2009) for assigning consecutive layer horizons, creating cross sections between boreholes and finally interpolating the solids, using bilinear interpolation. In total, 34 solid layers (Figs. 7b and 7c) were

generated. Careful examination of the stratigraphy of each well combined with comparisons of existing cross sections (Ariel and Consultores, 1996) were necessary to obtain a simplified, yet detailed, geologic representation of the basin. While preserving the general geologic topography, the 34 layers with 10 material types were further simplified to 14 layers with six material types. The final 2D mesh of 27,225 nodes (Fig. 7d), representing the horizontal extent of the simulation domain, was generated with a mesh refinement around the location of 167 representative wells. The topography of the 14 geologic horizons was sequentially extracted at each node by 15 2D mesh layers. The 3D mesh (Fig. 7f) is created by superposing the 15 2D mesh layers in the 3rd dimension (Fig. 7e). The 3D mesh has a total of 408,375 nodes and 760,284 elements.

### 3.4.2. Calibration and validation

The calibration process was done using the trial-and-error procedure. Hydraulic head and compaction were mostly solved by calibrating specific storage ( $S_s$ ) and skeletal specific storage  $S'_{ske}$ . Hydraulic conductivity ( $K$ ), and locations and intensity of pumping were also varied.

#### a) Groundwater flow model

Extensometer-1 and multilevel monitoring wells PL-201 and PL-205 (Fig. 10b) were the principal control piezometers selected for calibration of the hydraulic parameters. In addition to these monitoring wells, the 48 other multilevel monitoring wells (CONAGUA, 2008), dispersed throughout the center of the valley were used to simulate, as close as possible, the hydraulic behavior of the piezometric surface of the valley between 1969 and 2008. A higher grid resolution was placed on the industrial corridor where a large portion of the pumping, largest drawdowns, and subsidence is observed. Seasonal head variations could be of interest; however, considering that the groundwater levels are in a steady decline, only yearly data have been considered.

Yearly total pumping was estimated in 5–15 year increments. The total pumping rate of the entire valley (based on Calderhead (2009)), however, remained constant for all simulation, thus increasing pumping in one well, involved decreasing pumping in another well. The simulated drawdown at Extensometer-1, in addition to observed drawdowns at PL-201, PL-205, and Extensometer-1 is shown in Fig. 11. The evolution of the observed piezometry is reasonably reproduced by the model.

Specific storage ( $S_s$ ) values were calibrated to fit hydraulic head observations from multi-level piezometers as well as drawdown observed throughout the Toluca Valley. Increasing the specific storage values of the non-clay layers by an order of magnitude greater than field observations significantly improved the calibration of the model parameters. The specific storage values shown in Table 1 are the final values used for the simulations. Actual field values for  $S_s$  are approximately an order of magnitude lower (Ariel and Consultores, 1996; Lesser and Asociados, 1992).

Hydraulic conductivity values were modified slightly from field observations although their impact was not significant. It should be noted that the HGS-compaction model uses an uncoupled approach. Using uncoupled formulations causes a delay in the dissipation of the excess pore water pressure and consequently the appearance of the settlements (Ouria et al., 2007). The delay can be partly adjusted by modifying the hydraulic conductivity of clay layers. This delay cannot be adjusted completely by model calibration because the trend of time-settlement curves resulted from coupled and uncoupled models are not the same (Ouria et al., 2007).

Parameters that were not modified during the calibration process include porosity, average layer thickness, fraction of compressible material, and total pumping. Although not varied, these parameters can have significant effects on total compaction and could greatly influence final results.

## b) Aquifer-system compaction model

The principal control points compaction selected for calibration of the compaction parameters were Extensometer-1 and Extensometer-2, where detailed field compaction data was monitored, and the Pecuario well, a region with high subsidence rates measured by InSAR.

Using clay layer thicknesses (Figs. 5 and 10a), interferograms (e.g., Fig. 10b), pumping data (IMTA, 2003) (e.g., Fig. 10a) and hydraulic head measurements,  $S'_{ki}$  can be constrained for an individual layer  $i$ , belonging to a system of  $N$  layers.  $S'_k$  represents the skeletal storage coefficient of the entire aquifer system of  $N$  layers at a given location on the  $xy$  plane, and is given by:

$$S'_k = \sum_{i=1}^N S'_{ki} = \sum_{i=1}^N S'_{ski} b_i, \quad (5)$$

where  $b_i$  is the thickness of layer  $i$ .

Using data obtained from borehole logs, the fraction of compressible interbeds ( $\lambda_i$ ) can be estimated for all  $N$  layers (Table 1). A layer with no clay content is assigned a value of 0, conversely a layer with pure clay is assigned a value of 1. Assuming the given fraction of compressible interbeds for each layer, it is then possible to estimate  $S'_{sk}$  for individual clay layers ( $S'_{ski}$ ) (Eq. 5). For more details, the reader is referred to Calderhead (2009).

The few available compressibility indices (e.g., Calderhead (2009)) were used to derive clay compressibility ( $\bar{\alpha}$ ). These in turn helped calibrate inelastic skeletal specific storage coefficients ( $S'_{skv}$ ). See Calderhead et al (2011) and Gambolati and Teatini (2019) for a summary of the development of Eqs. discussed in this section. Additionally, the borehole logs, clay compressibility data from the Toluca aquifer system (UAEM, 2007) and empirically derived compressibility tables (de Marsily, 1986) assist in assigning  $S'_{sk}$  values to the layers. Only layers with clay content are considered compressible and all other layers are considered to have negligible compressibility.

Referring to Fig. 5 and Table 1, of the 14 model layers of material, the most influential layers in terms of compressibility are model layers 1 and 9. The others layers are considered to either be of negligible compressibility or to have a thickness too small to have a significant impact. Field data is not available for zone H, shown in Fig. 10B, however the InSAR data is useful in constraining  $S'_{ski}$  for this zone: although there is a high aggregate clay thickness and significant groundwater pumping (Fig. 10A) in zone H, all usable interferograms from 1996 to 2008 show very little to no subsidence in this zone. Observing Fig. 5 further, we notice that the thickness of clay layer 3 (Layer 9 of the model) is significant (40–80 m) in zone H, implying that the  $S'_{ski}$  value for this layer is most likely small and that layer 1 has the highest  $S'_{ski}$  and is the dominant compressible layer in this region. This is examined further in the discussion section.

Thus the large majority of the compaction, and total  $S'_{sk}$  (Eq. 5), measured by InSAR is attributed to model layer 1 (clay layer 1). By using the 3D geological model, pumping occurrences, and D-InSAR results, we are able to isolate the most compressible clay structure and assign more probable values to individual layers. Thus the uncertainty associated with the estimation is reduced to better constrain the  $S'_{sk}$  values.

Thus,  $S'_{skv}$  values (Table 1) were calibrated to fit compaction as measured by InSAR and Extensometer-1 and Extensometer-2.  $S'_{skv}$  was fine tuned to match the observed field compaction. Uncertainty remains in the estimate for the value of  $S'_{sk}$  partly because several other parameters are not fully certain (e.g., clay layer thicknesses and pumping). Elastic skeletal specific storage  $S'_{ske}$  values were generally assigned values in the range of half an order to one of magnitude lower than the  $S'_{skv}$  for the corresponding layer (Table 1). The parameter values in Table 1 for  $S'_{ske}$  and  $S'_{skv}$  are the final calibrated values used in the final simulation.

The comparison between the observed and simulated compaction seems adequate for the period of measured compaction at Extensometer-1, Extensometer-2 and the Pecuario well (Figs. 12 and 13). From December 2006 to July 2008, a pressure transducer at Extensometer-1 measured the hydraulic head every 12 h. From Fig. 12, it is seen that approximately 1 m of drawdown leads to 1 cm of compaction.

## 6. Results

### 6.1 Groundwater budget in the Toluca basin

Using HELP3, the average recharge for the Toluca basin in the past 35 years is estimated at 376 million cubic meters per year ( $Mm^3/year$ ). Fig. 8 illustrates the distribution of the average annual recharge rates in the Toluca Valley (mm/year), which was obtained from the HELP analysis using climate data from 1969 to 2000. When considering climate change predictions, by 2050 the average scenario projects recharge to decrease by 15  $Mm^3/year$ , and in a worst case scenario up to a maximum decrease of 88  $Mm^3/year$ . Groundwater pumping has increased steadily since 1970 and is expected for 2010 at 495  $Mm^3/year$ . Although the Toluca Valley's non-renewable water resources are being exploited at worrying rates, 38% of the groundwater resources are still being exported out of the basin. Inter-basin water transfer and growing local demand is having detrimental effects on the groundwater supply of the Toluca Valley.

This detailed assessment of two of the most important components of the water cycle (recharge and discharge) clearly shows that the decreasing water availability in the Toluca basin is due mostly to groundwater pumping (Fig. 9). To a lesser degree, climate change may play a role in the increasing deficit. The analysis shows that the current groundwater pumping is not sustainable. The current average deficit expected for 2010 is estimated at 172  $Mm^3/year$  with average projections increasing to over 292  $Mm^3/year$  by 2050 (Calderhead et al., 2012a, 2012b). This study of two of the most important components of the water cycle (recharge and discharge) clearly shows that the decreasing water availability in the Toluca basin is due mainly to anthropogenic effects and that the current pumping rates are not sustainable. The current deficit can be considered problematic and projections based on expected water consumption and climate change reinforce the need for management of the water resources to be addressed.

Based on the above analysis, Calderhead (2009) shows that there has been a water budget deficit in the Toluca Valley since the mid 1960s (Fig. 6) and this deficit continues to increase with time. Considering the increasing deficit within the basin, it was determined that over a long time (>10 years), seasonal head fluctuations did not have a significant impact on the total subsidence. Therefore, only yearly, as opposed to monthly or daily, recharge, discharge, and budget deficits were used for the simulations. With the assumption of the increasing deficit, subsidence (not uplift or clay expansion) is the dominant process and therefore more importance is given to the inelastic skeletal specific storage  $S'_{skv}$  as opposed to the elastic skeletal specific storage  $S'_{ske}$ .

## 6.2 Aquifer-system compaction and land subsidence

For the present study, Fig. 10b suggests that there is very limited interferometric coherence, or detectable surface movement, in the North-East and South-West corners, thus limiting its usefulness. However, usable results are obtained throughout the central part of the valley, where subsidence is the greatest. For the 70 day period between December 5<sup>th</sup> and February 13<sup>th</sup>, zones A through G are 'hotspots' with very clear subsidence patterns observed. If one observes the zoom on zone A (Fig. 10b), two color cycles (clockwise: yellow–blue–red; see legend of Fig. 10b) are observed and represent a total subsidence of 56 mm for the given period. This translates to subsidence rates of 28 cm/year.

Three locations in the industrial corridor, where drawdown has been monitored over a 40-year period and noticeable subsidence is observed are discussed (see Fig. 10a for locations): Extensometer-1 (Fig. 12), Extensometer-2, and the Pecuario well location (Fig. 13). Two of the three observation points have 2 years of extensometer data. Due to delays in obtaining subsidence maps, only D-InSAR data is available for the Pecuario well location; on-site surveys at this location are not available. The nearby monitoring wells, PL-201 and PL-205 (refer to Fig. 10b for location), are used for long term monitoring of hydraulic head or drawdown at an approximate depth of 150 m.

Although most of the D-InSAR data available for the Toluca Valley are from 2003 to 2008, one D-InSAR pair was obtained from the 1996 ERS-1 archives. The simulated compaction rates in 1996 at Extensometer-2 and the Pecuario well agree with the subsidence map generated with the ERS-1 sensor images (Fig. 13). Between 1996 and 2008 a total of 30 cm of subsidence is estimated at the Extensometer-1 and Extensometer-2 locations. While for the same time span, up to 80 cm of compaction is estimated at the highly compressible Pecuario well location.

The Extensometer-2 data slope (Fig. 13) coincides relatively well with the D-InSAR results and the numerical model. The magnitude of subsidence is similar to Extensometer-1's values with approximately 9 cm of compaction between November 2003 and May 2008. Considering the proximity of Extensometer 2 to Extensometer 1, hydraulic head is assumed to decrease at a rate similar to that observed at Extensometer-1 (Fig. 12). Considering the similar head decline at both locations, and that compaction magnitudes are similar for both locations—approximately 1 cm/year (Figs. 12 and 13); the total skeletal specific storage values are also assumed to be similar in this area.

Compaction and therefore skeletal specific storage ( $S'_{sk}$ ) appears higher at the Pecuario well location (Fig. 13) because the same amount of drawdown in this region (1 m) produces more compaction (8 cm) than elsewhere. According to the D-InSAR results, the Pecuario well location has had over 37 cm of total subsidence between November 2003 and May 2008. This point is close to the area where the highest subsidence rates are detected and it is estimated that the maximum total subsidence in the valley for the same period is in the order of 40 cm or around 8 cm/year.

Figs. 12a and 12b show the HGS compaction result superimposed on a D-InSAR subsidence map for the period from December 5<sup>th</sup> 2007 to May 28<sup>th</sup>, 2008. Simulations do not exactly match subsidence occurrences; however the region of maximum subsidence is in the same location for both methods. Magnitudes are slightly higher with D-InSAR, possibly because the measurements were taken during the dry season, when maximum drawdown and subsidence occurs. Seasonal compaction patterns could have been simulated, however, since there is a growing groundwater deficit over a 50 year period, subsidence occurrences on a larger time scale were preferred.

The groundwater deficit in the valley first occurred in the mid 1960s and has increased steadily ever since. From the simulations, minor compaction occurrences are observed in 1963 (Fig. 15) and total compaction reaches 2 m by 2009 (Fig. 16). As can be seen from Figs. 10–13, the simulation results agree reasonably well with the measured compaction occurrences between 2003 and 2008.

There is a lack, however, of regional subsidence data before 2003 with only a handful of studies examining subsidence occurrences in the Toluca Valley over the past 40 years (Consultec, 1978; Figueroa-Vega, 1990, 2004). These studies are mostly limited to the formation of fractures and none examine regional subsidence. Nevertheless, assuming the model is representative of the groundwater budget and material properties before 2003, it is estimated that the model is also representative of the subsidence occurrences before 2003.

The simulation results agree with the increased pumping over time, the subsidence occurrences have proportionally increased and are located in areas where compressible clay thickness is high (Figs. 10a, 15 and 16). Maximum subsidence rates are variable in space, time, and magnitude. The maximum rates depend on the geological context, the pumping rates, and the season, and even the year. There can be more subsidence induced in the dry period and less in the wet period. During the dry period, rates are as high as 30 cm/year (over a 5 month period). The maximum subsidence found in the Toluca Valley, near the Pecuario well location, considered a region with very high subsidence rates, with InSAR measurements over a four year period, indicate an average maximum yearly compaction of approximately 8 cm/year (Fig. 13).

## 7. Characterization of regional land subsidence

Limitations exist for the new HGS-compaction numerical model in representing subsidence. Both the solution approach and the use of representative data are major factors in obtaining reliable model results. However, the rapid decrease in hydraulic head in 2008 (Fig. 12) followed 4–5 months later by a rapid compaction rate can lead one to think that the compaction delays in the Toluca valley system are relatively fast compared to other systems (e.g., Mexico City), thus, based on the limited data, an instantaneous compaction representation for the Toluca Valley is acceptable. It should also be noted that what has been defined as clay layers in the model setup often implies interlayering with coarse alluvial deposits, often with relatively thin clay layers, implying that the drainage of the pore fluid to the surrounding aquifer can be relatively fast. A longer time span of compaction data coupled with hydraulic head information would enhance the understanding of the clay behaviour.

Using the linearized form of the constitutive law introduces representation errors. Leake and Prudic (1991) have estimated the error of this method by comparing the linearized equations of computed compaction with a more complex treatment of computed compaction using  $S'_{skv}$  proportional to  $\sigma'_{zz}$ . Their results indicate that using the linearized form overestimates compaction by approximately one-half the percentage increase in effective stress.

In that context, the new numerical model has helped in reproducing subsidence of the Toluca Valley. The new HGS-compaction code gives very reasonable estimates for instantaneous subsidence in confined aquifers; however there is room for improving the estimates and future work could include adding aspects such as dependence on hydraulic conductivity (e.g., Rudolph and Frind, 1991), stress dependent storage properties (e.g., Helm, 1976), time delays (e.g., Hoffmann et al. (2003a); Hoffmann et al. 2003b), effects of moving water tables (e.g., (Leake and Galloway, 2007; Liu and Helm, 2008), and extending to a 3D representation of deformation (e.g., Burbey and Helm (1999); Burkey (2001, 2005); Hsieh (1996); Lewis and Schrefler (1978); Safai and Pinder (1979)). One interesting new approach might include modeling approaches where local-scale and Biot-type models could be embedded in a simpler regional-scale model.


Hydraulic head variations in the Toluca Valley over the past 40 years are proof that there is a groundwater budget deficit (Fig. 9) and that the problem is not reversing itself. In terms of subsidence in the industrial corridor, the model shows up to 2 m of compaction occurring over the last 50 years. With the steady increase in groundwater deficit in the basin, an increase in the extent and magnitude of regional subsidence is observed from 1952 to 2009.



Although it represents a significant portion of total pumping in the Toluca Valley, the Lerma Pumping System is almost entirely situated in areas with limited clay content (Figs. 2 and 5a). Thus even with the large volumes of water extracted from these areas, there is only limited compaction in its vicinity. The impact of the Lerma Pumping is seen more as a regional problem affecting the deficit of the basin.

The extensive groundwater level monitoring system has been in place in the Toluca Valley since the late 1960s, yet more detailed information on the underlying geologic parameters would greatly enhance the predictive capability of the numerical model. A better 3D geological model could be achieved by including more borehole logs and consolidation tests. According to the InSAR results and the numerical model, it appears that most of the compaction is occurring in the upper 120 m of the aquifer. To enhance confidence, additional extensometers reaching immobile bedrock would increase our confidence in subsidence measurements at specific locations. Benchmarks should also be used to monitor the subsidence. As Aslan et al. (2019) and Castellazzi et al. (2017) have shown, recent advances in interferometry (PSI, SBAS and LiDAR) can be used to improve the assessment and analysis of aquifer-system compaction. Additionally, a more detailed census on the groundwater pumping tendencies occurring in the Toluca valley would enhance the understanding of groundwater flow. Seasonal subsidence information could be of interest, however, considering that the groundwater levels are in a steady decline, only yearly data has been considered. In summary, measuring and monitoring subsidence is critical to constrain analyses and forecast of future subsidence.

As noted by Calderhead et al. (2010) in their D-InSAR study of the Toluca Valley, maximum subsidence rates depend on the geological context, the pumping rates, and the season. There can be more subsidence induced in the dry period and less in the wet period. Some regions show high rates a given year and slower rates the following year, assuming constant or increasing pumping rates, this phenomenon is possibly due to the geological context. The maximum subsidence rates are therefore often variable in space, time, and magnitude. Maximum yearly subsidence, found in zone E (Fig. 10), over the period from 2003 to 2008 is around 10 cm/year.

It is found that the upper clay layer of the aquifer system is the most compressible unit. This information assists in assigning better estimates of the  $S'_{sk}$  values to the system. The low value of  in zone H (Fig. 10), mentioned in the calibration section, could be explained by the fact that older and deeper clays of clay layer 3 tend to be less compressible than more recent clays in layer 1. This in turn could explain why the extensometers readings, with data from the top 120 m of the system, coincide with the InSAR results and show that the large majority of compaction is occurring in the upper portion of the aquifer.

The large majority of the compaction, and total  $S'_{sk}$  (Eq. 5), measured by InSAR is attributed to model layer 1 (clay layer 1). By using the 3D geological model, pumping occurrences, and D-InSAR results, we are able to isolate the most compressible clay structure and assign more probable values to individual layers. This indicates that, the uncertainty associated with the estimation is reduced to better constrain the  $S'_{sk}$  values.

While not discussed in detail, the D-InSAR data was very useful, especially in locating areas with significant subsidence and extracting the specific storage ( $S'_{sk}$ ) values from individual layers. A hybrid approach using PSI, Small SBAS and conventional InSAR has a large potential for mapping subsidence. The study would have been very difficult to undertake without the satellite data. With a steady increase in the number of InSAR capable satellites being launched, more data and software will likely become available. Although several factors influence the suitability of InSAR use for deformation mapping, the usefulness of InSAR is bound to improve.

Based on the available data, the results appear to be reliable. The multidisciplinary approach of using a 3D geological model, pumping estimates, hydraulic head measurements, D-InSAR, and extensometers to constrain the numerical model enables a very reasonable representation of the system. These efforts generally seek to obtain some level of sustainable use of the resources, which typically is best defined by the resource managers in concert with local stakeholders, and takes the form of maximizing beneficial uses while minimizing perceived unacceptable consequences.

**Acknowledgements** We are thankful to the Ministère des Relations Internationales du Québec, INRS-ETE, NSERC (a discovery grant held by Richard Martel and René Therrien), the Autonomous University of the State of México (UAEM), COMECYT, CONACyT, AUCC/IDRC, and the Ministère de l'Éducation du Québec for their financial support. We are appreciative of Sergio Murillo from the Commission National del Agua for logistical support on the field. We are grateful also to the Canadian Space Agency and the Geological Survey of Canada for providing the RADARSAT-1 data. We acknowledge the European Space Agency's contribution for providing ERS and ENVISAT ASAR data at cost of reproduction under project C1P 3821.

## References

- ADWR, 2011. Maps of land subsidence areas in Arizona: Scottsdale subsidence feature. ADWR, Phoenix, AZ. [http://www.adwr.state.az.us/azdwr/Hydrology/Geophysics/documents/ScottsdaleArea2004to2010\\_8x11.pdf](http://www.adwr.state.az.us/azdwr/Hydrology/Geophysics/documents/ScottsdaleArea2004to2010_8x11.pdf). Cited 31 May 2011.
- Amelung F, Galloway DL, Bell JW, Zebker HA, Lacznik RJ, 1999. Sensing the ups and downs of Las Vegas: InSAR reveals structural control of land subsidence and aquifer-system deformation. *Geology*; 27:483–6.
- Ariel and Consultores, 1996. Estudio de Simulación Hidrodinámica y Diseño Optimo de las Redes de Observación de los acuíferos de Calera, San Luis Potosí y Toluca (Tomo 3: Acuífero de Toluca), Comisión Nacional del Agua, México, DF, 308 p.
- Gokhan Aslan G, Cakir Z, Lasserre C, 3 Renard F, 2019. Investigating subsidence in the Bursa plain, Turkey, using ascending and descending Sentinel-1 Satellite data. *Remote Sens.* 2019, 11, 85; doi:10.3390/rs11010085.
- Berardino P, Fornaro G, Lanari R, and Sansosti E, 2002. A New Algorithm for Surface Deformation Monitoring Based on Small Baseline Differential SAR Interferograms. *IEEE Transactions on Geoscience and Remote Sensing* 40: 2375–2383. doi:10.1109/TGRS.2002.803792.
- Biot MA, 1941. General theory of three dimensional consolidation. *J Appl Phys* 194,12:155–64.
- Bonsignore F, Bitelli G, Chahoud A, Macini P, Mesini E, Severi P, Villani B, Vittuari L, 2010. Recent extensometric data for the monitoring of subsidence in Bologna (Italy). In: Carreón-Freyre D, Cerca M, Galloway DL, Silva-Corona JJ (eds) Land subsidence, associated hazards and the role of natural resources development (EISOLS 2010). IAHS Publ. 339, IAHS, Wallingford, UK, pp 333–338.
- Burbey TJ, Helm DC., 1999. Modeling three-dimensional deformation in response to pumping of unconsolidated aquifers. *Env Eng Geosci*, 5:199–212.
- Burbey TJ, 2001. Stress–strain analyses for aquifer-system characterization. *Ground Water*, 39(1):128–136.
- Burbey TJ, 2005. Use of vertical and horizontal deformation data with inverse models to quantify parameters during aquifer testing. In: Zhang A, Gong S, Carbognin L, Johnson AI, editors. Land subsidence – Proceedings of the 7th international symposium on land subsidence, vol. 2. Shanghai, PR China: Shanghai Scientific and Technical Publishers, p. 560–569.
- Calderhead AI, 2009. Pumping effects on land subsidence: assessment using field data, remote sensing and numerical modeling. PhD thesis. Institut national de la recherche scientifique, Université du Québec, 314 p.
- Calderhead A, Martel R, Alasset P-J, Rivera A and Gárfias J, 2010. Land subsidence induced by groundwater pumping, monitored by D-InSAR and field data in the Toluca Valley, Mexico. *Canadian Journal of Remote Sensing (Best paper Award 2010)*, vol. 36, No. 1, p. 9-23.
- Calderhead A, Therrien R, Rivera A, Martel R and Gárfias J, 2011. Simulating pumping-induced regional land subsidence in a complex aquifer system. *Advances in Water Resources*, Vol. 34(1), pp. 83-97.
- Calderhead A, Martel R, Gárfias J, Rivera A and Therrien R, 2012a. Sustainable Management for Minimizing Land Subsidence of an Over-Pumped Volcanic Aquifer System: Tools for Policy Design. *Water Resources Management*, (ISSN: 0920-4741), vol. 26, No. 7, p. 1847-1864
- Calderhead A, Martel R, Gárfias J, Rivera A and Therrien R, 2012b. Pumping dry: an increasing groundwater budget deficit induced by urbanization, industrialization, and climate change in an over-exploited volcanic aquifer. *Environmental Earth Sciences Journal*, vol. 66, No. 7, p. 1753-1767.

- Chaussard E, Wdowinski S, Cabral-Cano E, Amelung F, 2014. Land subsidence in central Mexico detected by ALOS InSAR time-series. *Remote Sens. Environ*, 140, 94–106.
- CONAGUA, 2002. Determinación de la Disponibilidad de Agua en el Acuífero Valle de Toluca, Estado de México. Comisión Nacional del Agua, México, DF. 31 p.
- CONAGUA, 2006. Datos climatológicos, Servicio Meteorológico Nacional, Comisión Nacional del Agua, 345 p.
- CONAGUA, 2008. Registro de Lecturas Piezométricas por el Valle de Toluca, 157 p.
- CONAPO (2015). Delimitación de las zonas Metropolitanas de México 2015. Consejo Nacional de Población, 286 p.
- Consultec, 1978. Estudio del comportamiento de grietas en el valle del Alto Rio Lerma. Informes I-III, 275 p.
- Conway BD, 2016. Land subsidence and earth fissures in south-central and southern Arizona, USA, *Hydrogeol J* (2016) 24:649–655.
- de Marsily G, 1986. Quantitative hydrogeology. Groundwater hydrology for engineers. New York: Academic Press, 464 p.
- ETEISA, 1995. Estudio Para la Medición y Configuración Piezométrica de la Red de Pozos Piloto de la DGCOH en el Alto Lerma y Actualización y Digitalización del Plano Base de la Zona del Alto Lerma. Gobierno del Distrito Federal, Secretaria de Obras y Servicios (DGCOH), Contrato: 5-111-1-0182.
- ETEISA, 1997. Estudio de Evolución de Niveles Piezométricos en la Cuenca del Alto Lerma Para el Periodo 1985-1997: Informe Final. Gobierno del Distrito Federal, Secretaria de Obras y Servicios (DGCOH), Contrato: 7-CO4-1-0371.
- Ferretti A, Prati C and Rocca F, 2000. Nonlinear Subsidence Rate Estimation Using Permanent Scatterers in Differential SAR Interferometry. *IEEE Transactions on Geoscience and Remote Sensing* 38: 2202–2212. doi:10.1109/36.868878.
- Ferretti, A., C. Prati, and F. Rocca. 2001. "Permanent Scatterers in SAR Interferometry." *IEEE Transactions on Geoscience and Remote Sensing* 39 (1): 8–20. doi:10.1109/36.898661.
- Figuroa Vega GE, 2004. El agrietamiento de la ciudad de Toluca. Consejo consultivo de Agua, December, 85 p.
- Figuroa Vega GE, 1990. Estudio sobre el comportamiento reciente del acuífero de la ciudad de Toluca y su relación con el problema de agrietamientos de la zona poniente de la misma, CEAS, Estado de México, 235 p.
- Galloway DL, Hudnut KW, Ingebritsen SE, Phillips SP, Peltzer G, Rogez F, et al., 1998. Detection of aquifer system compaction and land subsidence using interferometric synthetic aperture radar, Antelope Valley, Mojave Desert, California. *Water Resour Res*, 34:2573–85.
- Galloway DL, Hoffmann J, 2007. The application of satellite differential SAR interferometry-derived ground displacements in hydrogeology. *Hydrogeol J* 2007;15(1):33–154. doi:10.1007/s10040-006-0121-5.
- Galloway D, Burbey TJ, 2011. Review: Regional land subsidence accompanying groundwater extraction. *Hydrogeol J* 19:1459–1486.
- Gambolati G, 1972. A three-dimensional model to compute land subsidence. *Bullet Int Ass Hydrol Sci*, 17:219–26.
- Gambolati G, Teatini P, 2019. Groundwater and land subsidence. An Evolving Platform for Groundwater Education and Practice. In Ebook, *An Evolving Platform for Groundwater Education and Practice*. Edited by John Cherry, Institute for Groundwater Research, University of Guelph.
- Gárfias J, Llanos H, Bibiano L, 2008. Uso Racional y Sostenible de los recursos hídricos del acuífero del valle de Toluca. *Revista Ciencia Ergo Sum*, Vol. 15–1, May–June 2008, pp. 61–72.

- Gobierno del Estado de México, 1997. Atlas Ecológico de la Cuenca Hidrográfica del Río Lerma; Tomo III (Impacto de las actividades productivas en el suelo) y (Un recurso escaso, valioso y necesario: El agua). Comisión Coordinadora para la Recuperación Ecológica de la Cuenca del Río Lerma, 138 p.
- GMS, 2009. GMS 6.5 User guide, GMS-Salt lake City, Utah, 2009, 475 p.
- Grupo Herram, 1992. Estudio Hidrogeológico Regional de Toluca e Ixtlahuaca, Tomo I: Informe. DCGOH, Contrato No: 3-33-1-0162.
- GTZ-CNA. 2004. Modelo de Simulación Hidrodinámica del Acuífero del Valle de Toluca, Estado de México. Deutsche Gesellschaft für Technische Zusammenarbeit -Comisión Nacional del Agua, 178 p.
- Hancox J, Gárfias J, Aravena R and Rudolph DL, 2010. Assessing the Vulnerability of over-exploited volcanic aquifer systems using Multiparameter Analysis, Toluca Basin, Mexico. *Environmental Earth Sciences*; Vol. 59(8), p. 1643-1660.
- Hanssen RF, 2001. Radar interferometry—data interpretation and error analysis. Kluwer Academic Publisher, 308 p.
- Helm DC, 1975. One-dimensional simulation of aquifer system compaction near Pixley, California, 1, Constant parameters. *Water Resour Res*, 11:465–78.
- Helm DC, 1976. One-dimensional simulation of aquifer system compaction near Pixley, California. 2, Stress-dependent parameters. *Water Resour Res*, 1(3):375–91.
- Hoffmann J, Galloway D, Howard AJ, 2003a. Inverse modeling of interbed storage parameters using land subsidence observations, Antelope Valley, California. *Water Resour Res*, 39(2):1231.
- Hoffmann J, Leake SA, Galloway DL, Wilson AM, 2003b. MODFLOW-2000 groundwater model – user guide to the Subsidence and Aquifer-System Compaction (SUB) Package: US Geological Survey Open – File Report 03-233, 46 p.
- Hoffmann J, Zebker HA, 2003c. Prospecting for horizontal surface displacements in Antelope Valley, California, using satellite radar interferometry. *J Geophys Res* 108(F1):6011. doi:10.1029/2003JF000055.
- Hsieh PA, 1996. Deformation-induced changes in hydraulic head during groundwater withdrawal. *Ground Water*, 36(6):1,082–9.
- IMTA, 2003. Censo del utilización del agua en el valle de Toluca. Instituto Mexicano de Tecnología del Agua, 247 p.
- INEGI, 1960. Censo general de población y vivienda, Instituto Nacional de Estadística, Geografía e Informática, 245 p.
- Leake SA, Prudic DE, 1991. Documentation of a computer program to simulate aquifer-system compaction using the modular finite-difference ground-water flow model: US Geological Survey Techniques of Water-Resources Investigations, Book 6, Chapter A2, 68 p.
- Leake SA, Galloway DL, 2007. MODFLOW ground-water model—User guide to the Subsidence and Aquifer-System Compaction Package (SUB-WT) for watertable aquifers: US. Geological Survey, Techniques and Methods 6-A23, 42 p.
- Lesser and Asociados, 1992. Estudio para el Diagnostico del acuífero del Valle de Toluca, para implementar la reglamentación de la extracción del agua subterránea, 325 p.
- Lewis RW, Schrefler B, 1978. Fully coupled consolidation model of subsidence of Venice. *Water Resour Res*, 14(2):223–30.
- Liu Y, Helm DC, 2008. Inverse procedure for calibrating parameters that control land subsidence caused by subsurface fluid withdrawal: 1. Methods. *Water Resour Res*, 44(W07423). doi:10.1029/2007WR006605.

- Liu, JC and DV, Griffiths DV, 2015. A general solution for 1D consolidation induced by depth- and time-dependent changes in stress, *Géotechnique*, 10.1680/geot.14.P.077, **65**, 1, (66-72).
- Nelson SA, Sanchez-Rubio G, 1986. *Trans Mexican Volcanic Belt Field Guide*. Volcanology Division, Geological Association of Canada, 108 p.
- Osmanoglu B, Dixon TH, Wdowinski S, Cabral-Cano E, Jiang Y, 2011. Mexico City subsidence observed with persistent scatterer InSAR. *Int J Appl Earth Obs* 13:1–12. doi:10.1016/j.jag.2010.05.009.
- Ouria A, Toufigh MM, Nakhaie A, 2007. An investigation on the effect of the coupled and uncoupled formulation on transient seepage using the finite elements method, *A. J Appl Sci*, 4(12), 950-956.
- Roctest Ltd, 2009. Instructor manual, Magnetic Reed Switch Probe Extensometer System Model R-4, 15 p.
- Rudolph DL, Frind EO, 1991. Hydraulic response of highly compressible aquitards during consolidation. *Water Resour Res*, 27(1):17–28.
- Rudolph DL, Sultan R, Garfias J, McLaren RG, 2006. Significance of Enhanced Infiltration due to Groundwater Extraction on the Disappearance of a Large Wetland System: Lerma River Basin, Mexico. *Hydrogeology Journal*, vol. 14 (1-2), pp. 115-130.
- Safai NM, Pinder GF, 1979. Vertical and horizontal land deformation in a desaturating porous medium. *Adv Water Resour*, 2:19–25.
- SRH, 1970. *Los acuíferos del alto Lerma* pub. Comisión hidrológica de la cuenca del valle de México, 66 p.
- Tessitore S, Fernández-Merodo, JA, Herrera G, Tomás R, Ramondini M, Sanabria M, Duro J, Mulas J & Calcaterra D, 2016. Comparison of water-level, extensometric, DInSAR and simulation data for quantification of subsidence in Murcia City (SE Spain). *Hydrogeology Journal*, 24, 727-747.
- Therrien R, McLaren G, Sudicky EA, Panday SM, 2009. User guide: hydrogeosphere – a three-dimensional numerical model describing fully-integrated subsurface and surface flow and solute transport, 430 p.
- Tomás R, Herrera G, Delgado J, Lopez-Sanchez JM, Mallorqui JJ, Mulas JA, 2009. ground subsidence study based on DInSAR data: Calibration of soil parameters and subsidence prediction in Murcia City (Spain). *Eng. Geol*, 111, 19–30.
- UAEM, 2007. *Compilation of clay compressibilities of the Toluca Valley, Mexico*, 57 p.
- Ye SJ, Xue XQ, Wu JC, Li QF, 2012. Modeling visco-elastic-plastic deformation of soil with modified merchant model. *Environ Earth Sci* 66:1497–1504.
- Zebker HA, Rosen PA, Hensley S, 1997. Atmospheric effects in interferometric synthetic aperture radar surface deformation and topographic maps. *J Geophys Res*, 102(B4): 7547–63.

**Table 1.** Description of calibrated material properties for the Toluca Valley to fit compaction as measured by InSAR and Extensometer-1 and Extensometer-2.

Layer number (From top to bottom)	Description	AT*	HC*	SS*	P*	F*	ES*	IS*
		$b$ [m]	$K$ [m/s]	$S_s$ [1/m]	$\theta$ [-]	$\gamma^*$ [-]	$S'_{skv}$ [1/m]	$S'_{skv}$ [1/m]
Layer 1	clays 1	45.9	2.0E-06	5.6E-06	0.40	0.7	9.2E-07	3.7E-06
Layer 2	sand and gravel	18.0	4.0E-04	1.2E-06	0.35	1.0E-04	3.6E-08	1.4E-07
Layer 3	fine grains	16.9	3.0E-05	1.4E-06	0.30	1.0E-04	8.4E-08	3.4E-07
Layer 4	clay 2	2.1	2.0E-06	1.7E-06	0.35	0.7	3.0E-07	4.2E-07
Layer 5	fine grains	17.1	6.0E-05	1.4E-06	0.35	1.0E-04	8.6E-08	3.4E-07
Layer 6	coarse grains	19.0	1.0E-03	1.2E-06	0.35	1.0E-04	3.3E-08	1.3E-07
Layer 7	sand and gravel	10.6	4.0E-04	1.1E-06	0.35	1.0E-04	2.1E-08	8.5E-08
Layer 8	volcanic solids	6.7	6.0E-04	1.0E-06	0.30	1.0E-04	1.7E-12	6.7E-12
Layer 9	clays 3	21.9	5.0E-07	5.6E-06	0.35	0.7	2.1E-07	4.4E-06
Layer 10	conglomerate	7.3	6.0E-05	1.0E-06	0.30	1.0E-04	1.8E-12	7.3E-12
Layer 11	sand and gravel	6.8	4.0E-04	1.1E-06	0.35	1.0E-04	1.4E-08	5.4E-08
Layer 12	clays 4	3.7	6.0E-06	1.9E-06	0.35	0.7	1.9E-07	7.5E-07
Layer 13	fine grains	9.8	6.0E-05	1.2E-06	0.35	1.0E-04	4.9E-08	2.0E-07
Layer 14	sand and gravel	2.0	4.0E-04	1.0E-06	0.35	1.0E-04	4.0E-09	1.6E-08
Zones A-G	High compressibility areas of layer 1	30	2.0E-06	4.4E-06	0.35	1.0E-04	1.0E-06	2.4E-06

\* AT: Average thickness, HC: Hydraulic Conductivity, SS: Specific Storage, P: Porosity, F: Fraction of compressible materials, ES: Elastic skeletal specific storage, IS: Inelastic skeletal specific storage.

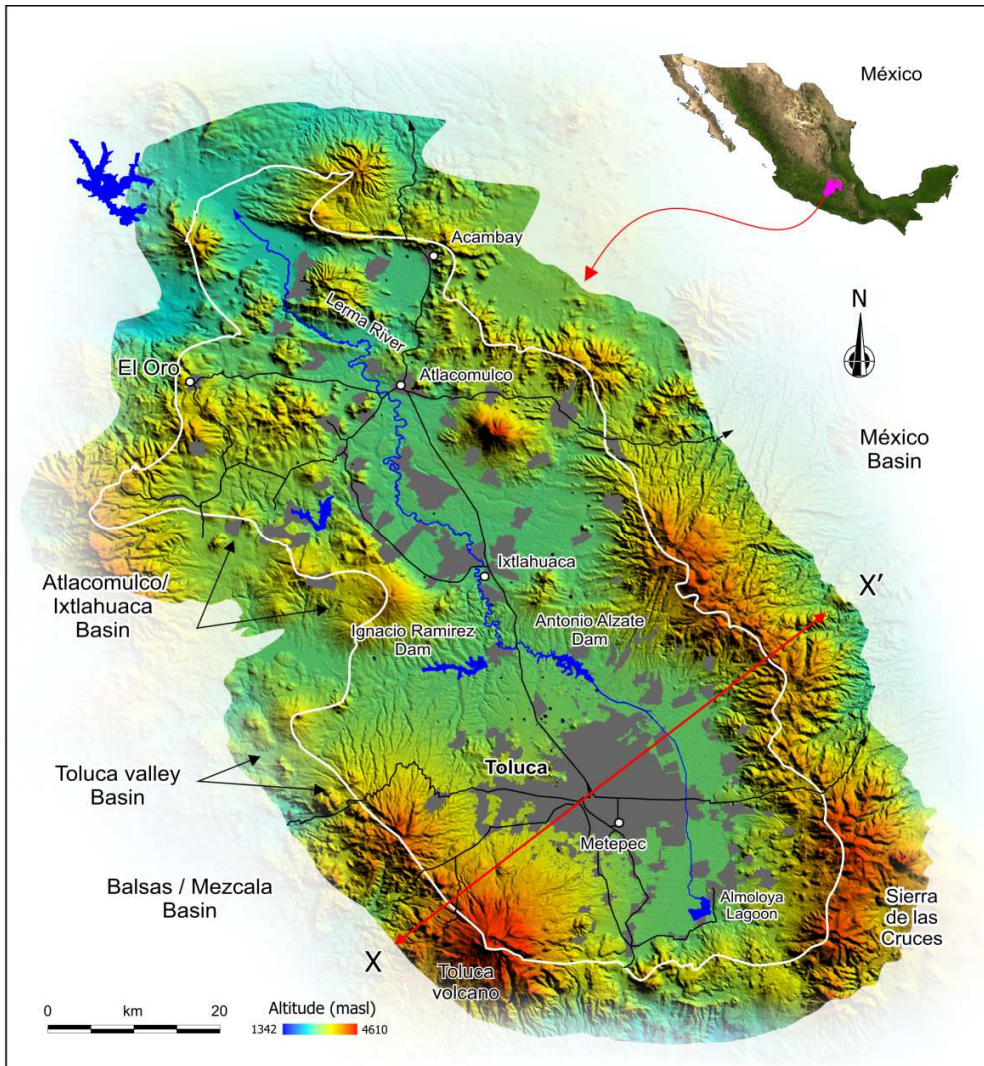


**Figure 1.** The setting of the Upper Lerma River Basin showing principal physiographic features and the extent of the Atlacomulco/Ixtlahuaca basin to the north and the Toluca basin to the south. Also shown are the neighboring basins and the location of the schematic stratigraphic cross-section X-X' shown in Figure 3.



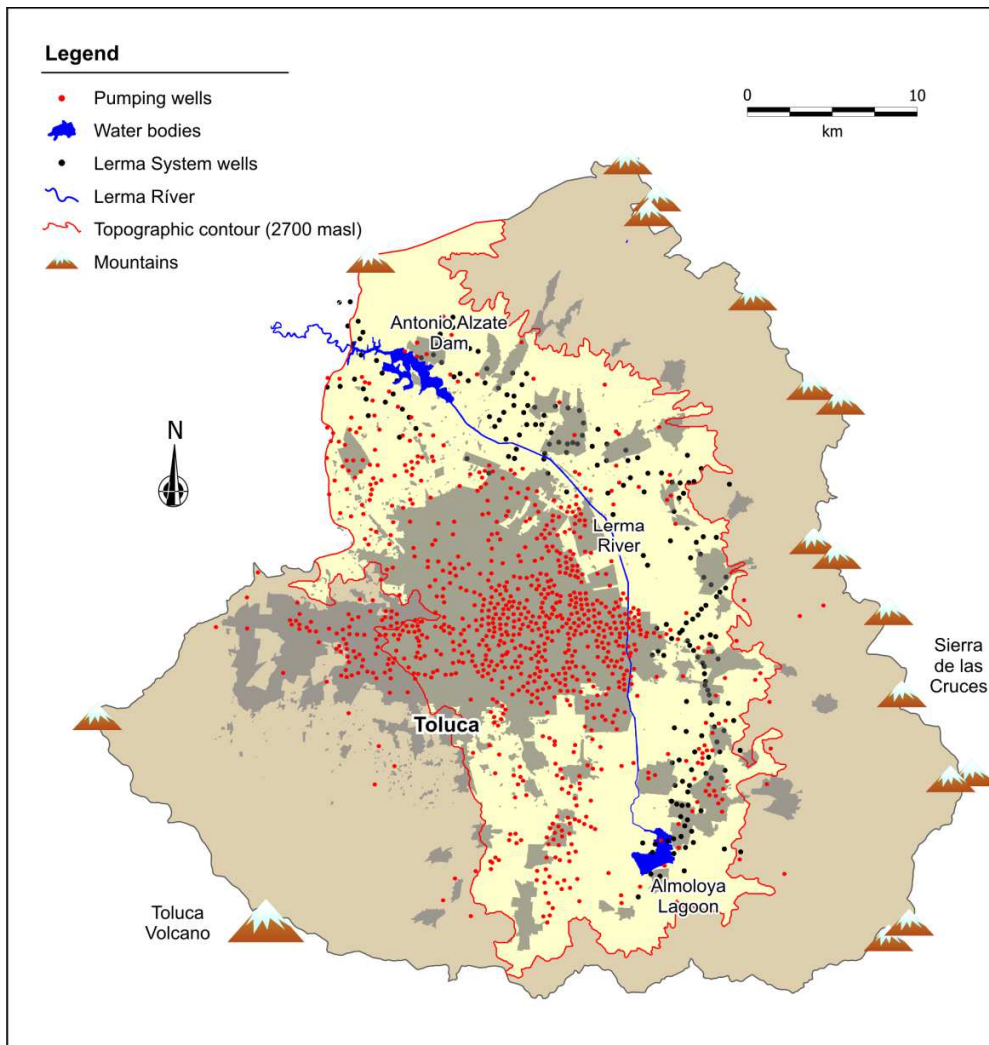


**Figure 2.** Map of the Toluca Basin showing principal surface water bodies and boundaries of the watershed. Also shown is the location of the 935 pumping wells, including the 230 Lerma system wells pumping water to the Mexico Basin, as well as the urban area for 2015 delimited using Landsat images.

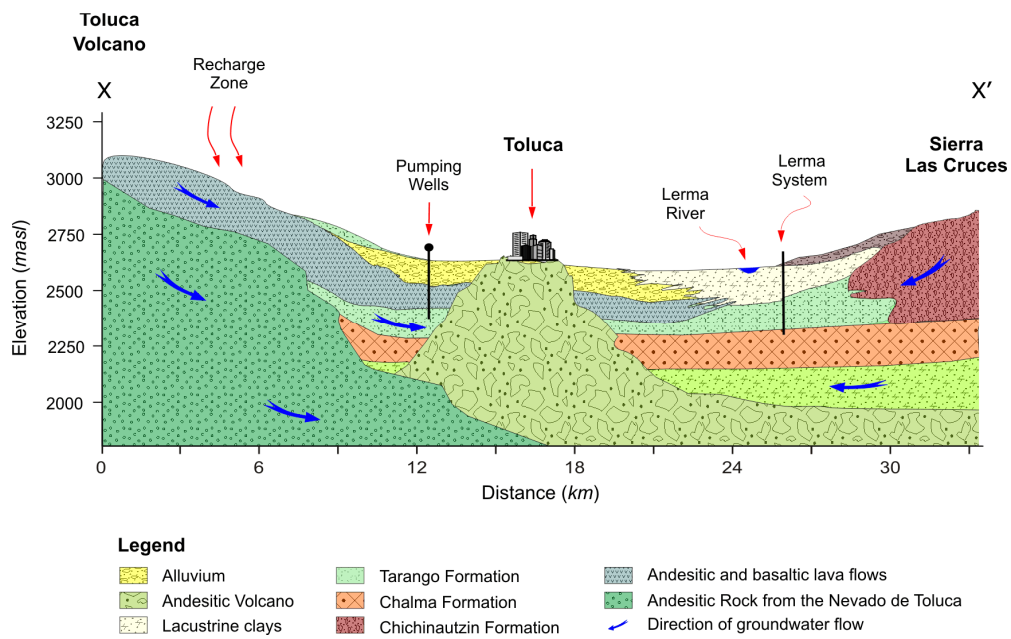


**Figure 3.** Schematic stratigraphic cross-section X-X' through the southern of the Toluca basin shown in Fig. 1. The location of the Lerma system and the flow directions of groundwater associated to recharge areas are also indicated in the diagram (modified from Rudolph et al. (2006) and Calderhead et al. (2011)).

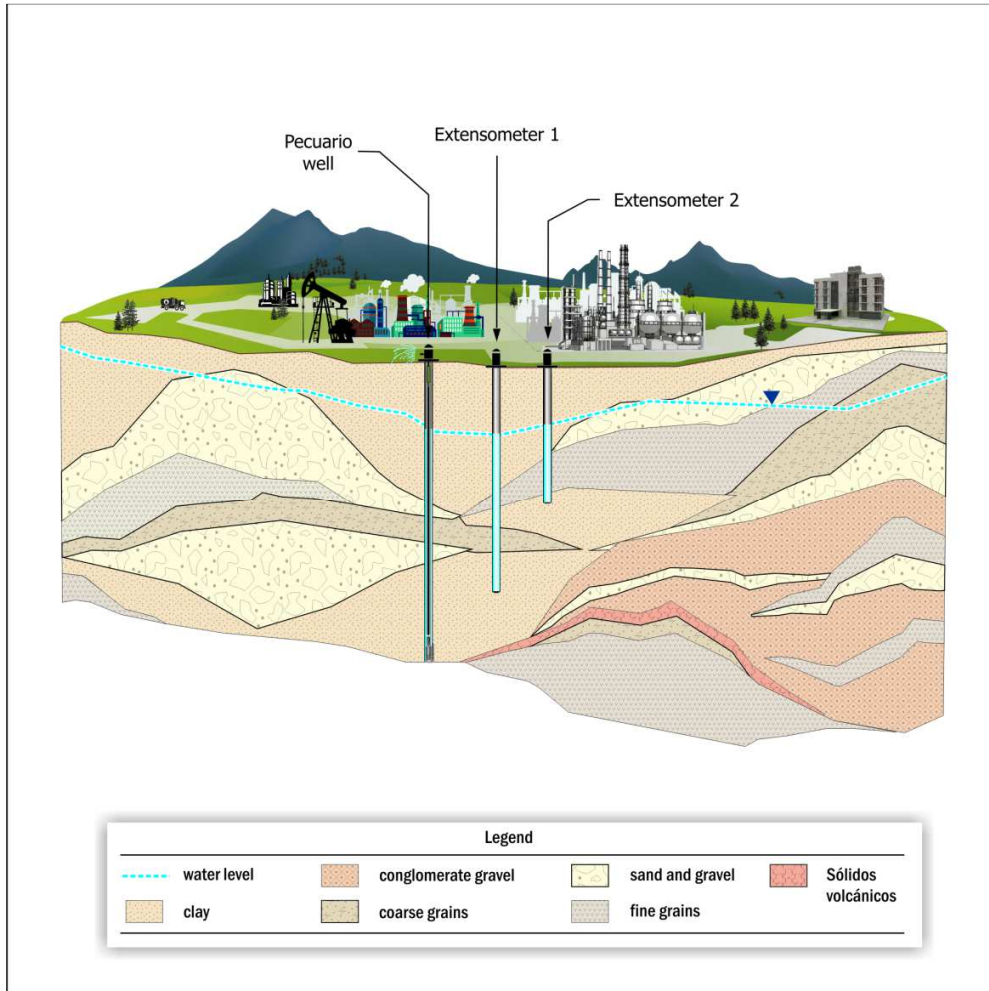


**Figure 4.** Three-dimensional schematic model of the industrial corridor study area showing the location of the observations points (Pecuario well, Extensometer-1 and Extensometer-2). Locations of observations points are placed in plain view on Figs. 10 and 14 (modified from Calderhead et al. (2011)).

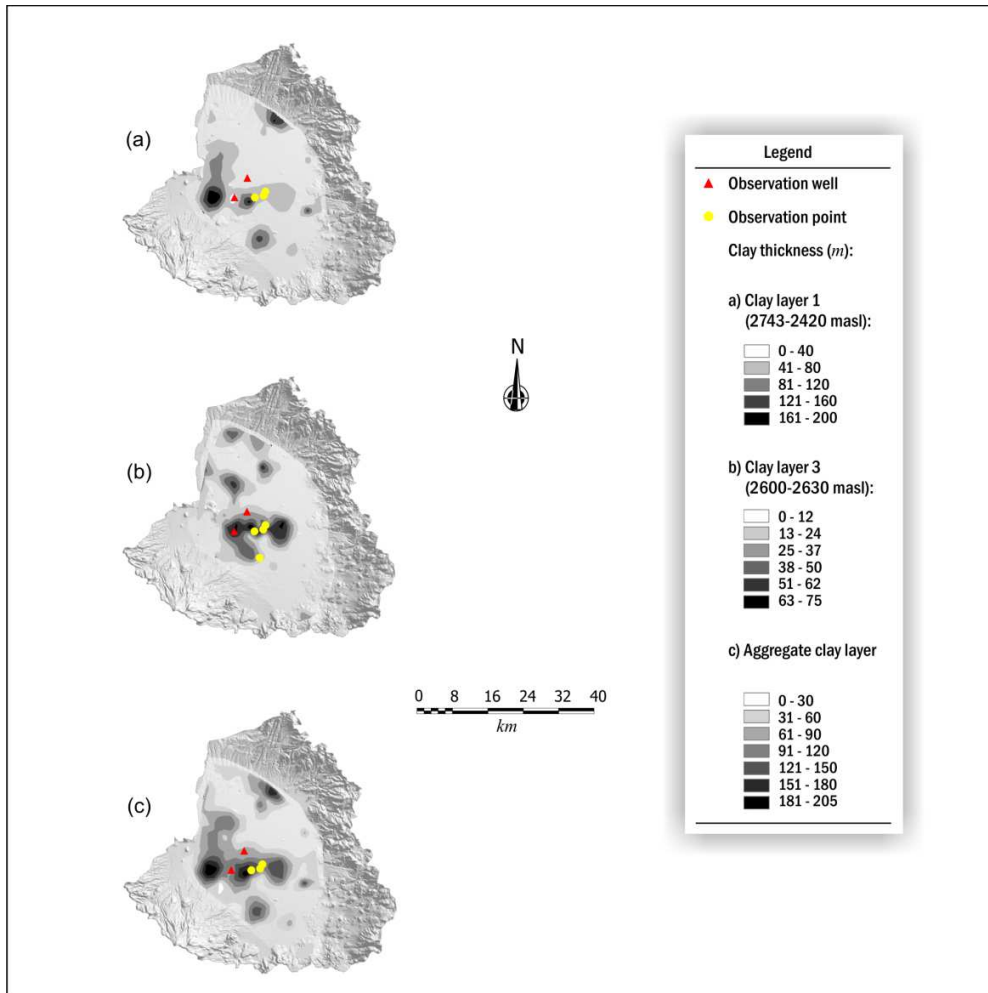


**Figure 5.** Spatial distribution of clay layer thickness in the Toluca Aquifer system (5a) and (5b) and aggregate clay thickness (5c). Clay layer properties are given in Table 1.

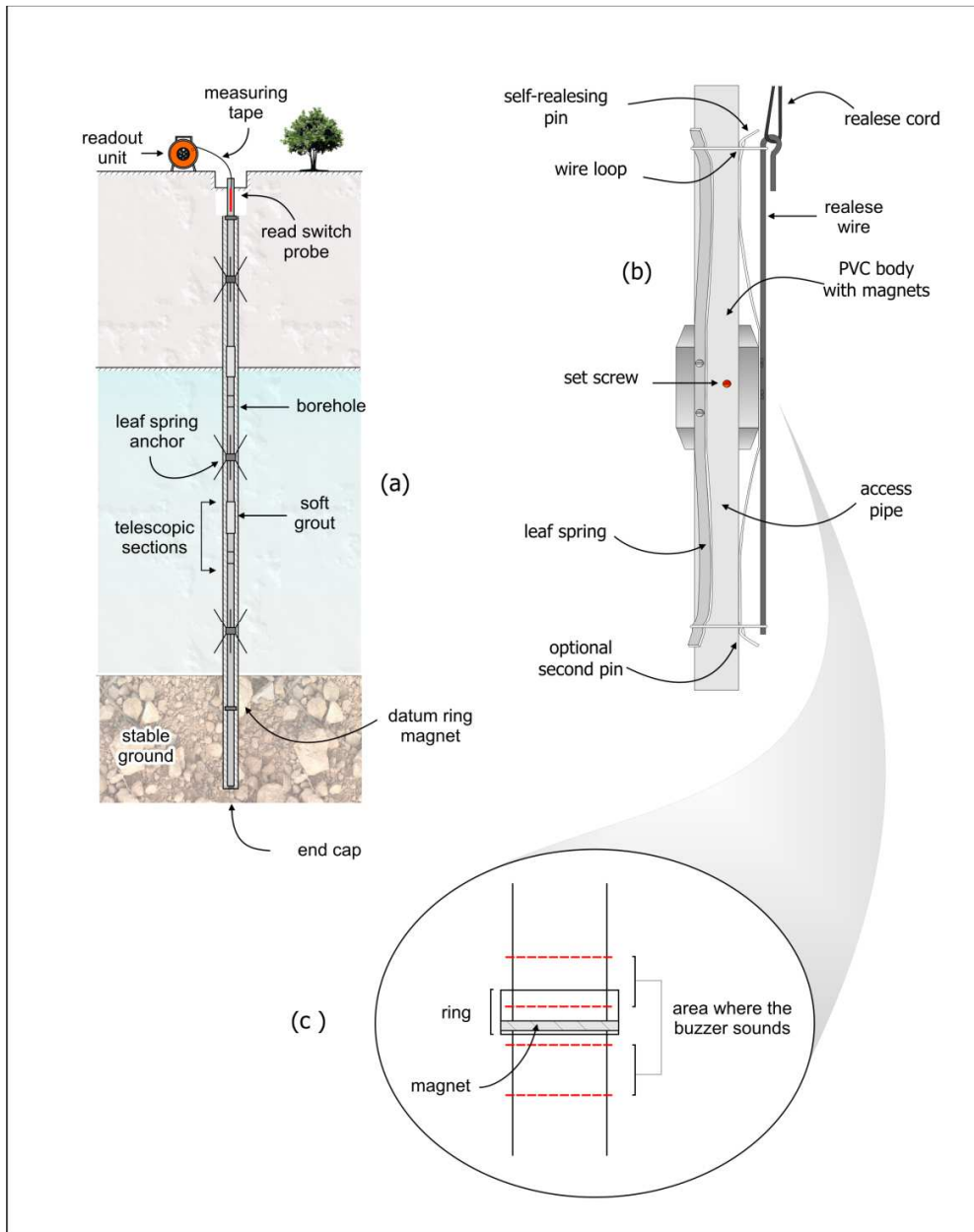


**Figure 6.** Schematic drawing of the magnetic probe extensometers installed in the Toluca aquifer system: (a) schematic diagram of the R-4 magnetic reed switch probe extensometer system; (b) leaf spring anchor containing the magnets; (c) sketch of sensitive areas to take readings.

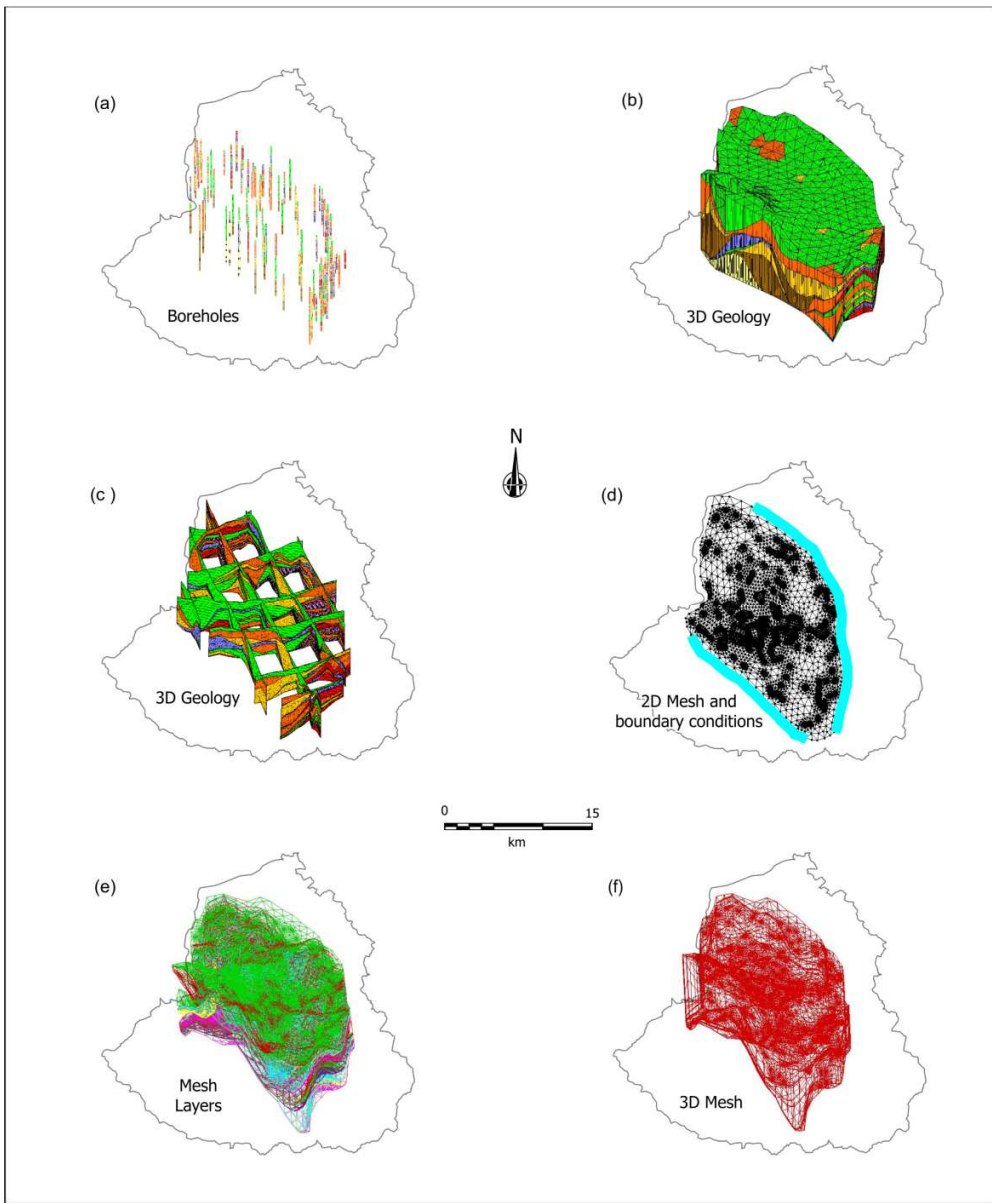


**Figure 7.** Processing chain for obtaining the 3D finite-element model domain. Boreholes (a) are used to generate 3D geology (b and c), then using the geologic layers and the 2D mesh (d), the topography of the geological layers are extracted (e). Finally the 3D mesh (f) is generated to obtain a representative regional model.

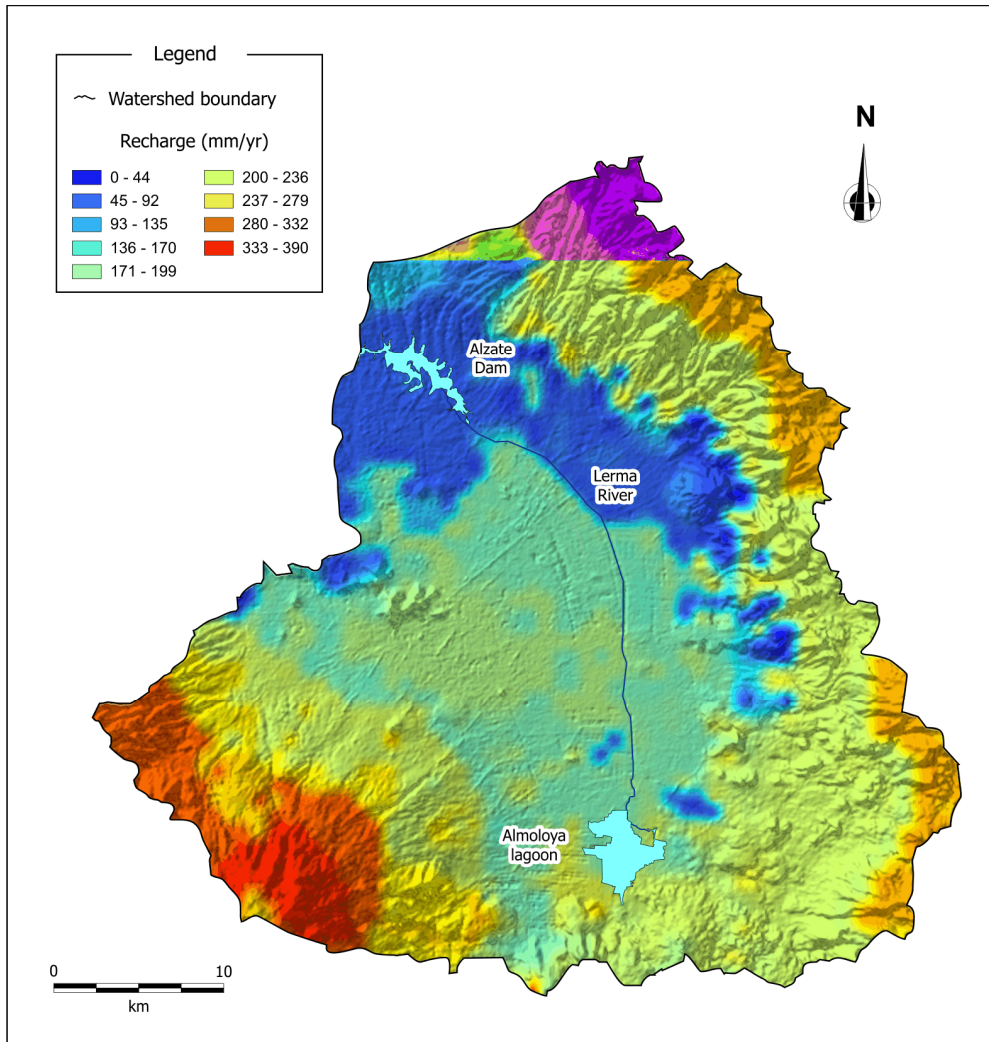


**Figure 8.** Spatially variable distribution of average annual recharge rates in the Toluca Valley (mm/year) obtained from the HELP analysis using climate data from 1969 to 2000 (modified from Calderhead et al. (2010)).

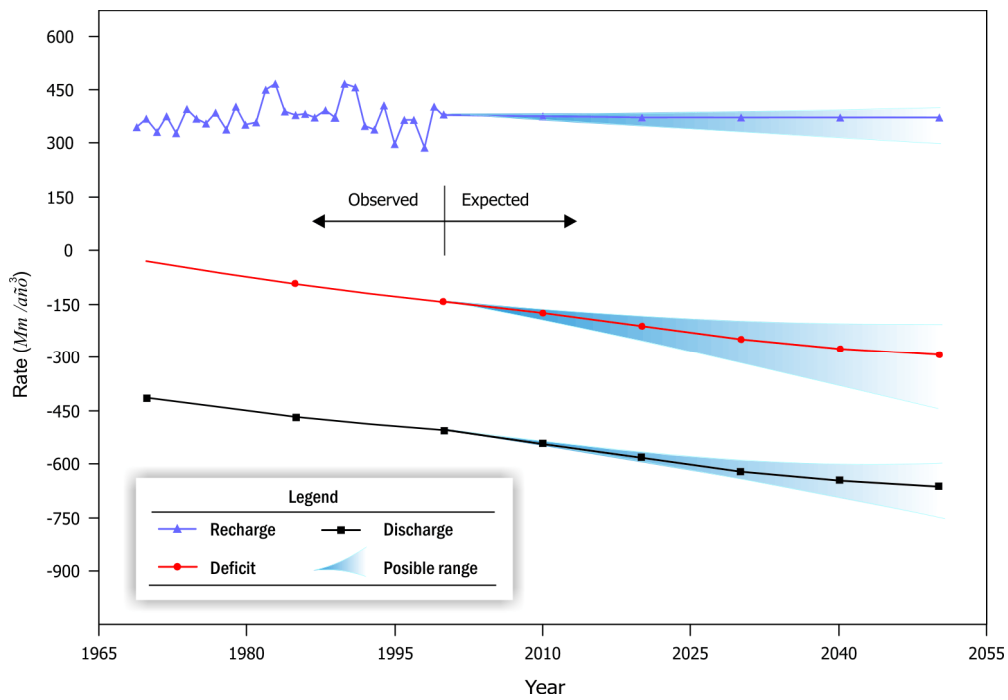


**Figure 9.** Observed and expected groundwater recharge, pumping and deficit from 1970 to 2050. Recharge values include induced recharge ( $R_{art}$ ). From 1969 to 1999 actual recharge values are shown; the average for that time period is estimated at  $376.2 \text{ Mm}^3/\text{year}$ . Recharge from 2000 to 2050 is based on the average value and Climate Change (CC) average variations (IPCC, 2007). Historical discharge is based on the literature and groundwater levels and future discharge is based on the projections discussed in “Total discharge  $Q_{out}$ ”. The deficit is the sum of the recharge and the discharge (modified from Calderhead et al. (2010)).



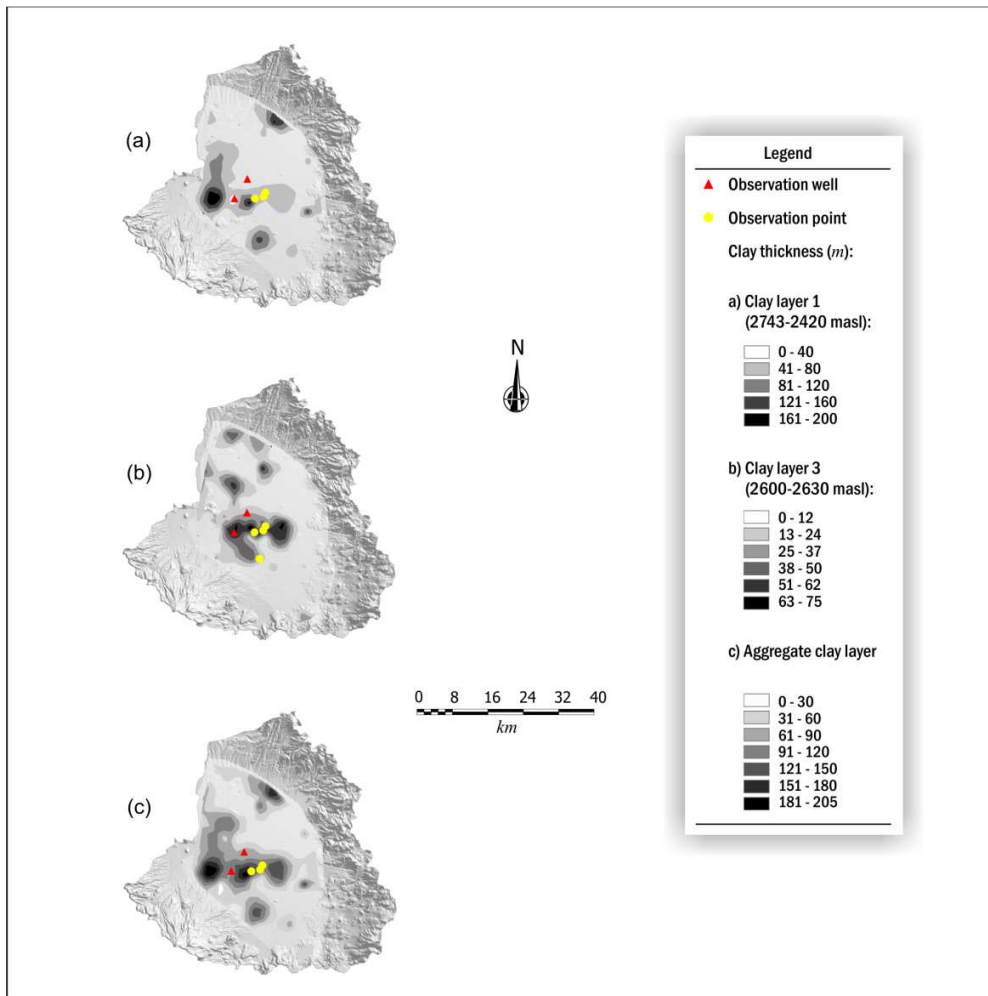


**Figure 10.** (a) Map of aggregate clay thickness and pumping well extraction rates; (b) Differential Interferogram of the Toluca Valley with a time interval of 70 days. ENVISAT ASAR images were acquired on December 5<sup>th</sup>, 2007 and February 13<sup>th</sup>, 2008. A blue–red–yellow cycle represents subsidence (2.8 cm), conversely blue–yellow–red would represent uplift. Lines of equal aggregate thickness (based on Fig. 10A) are also shown on the map. (For interpretation of the references to colour in this figure legend, the reader is referred to Calderhead et al. (2011)).

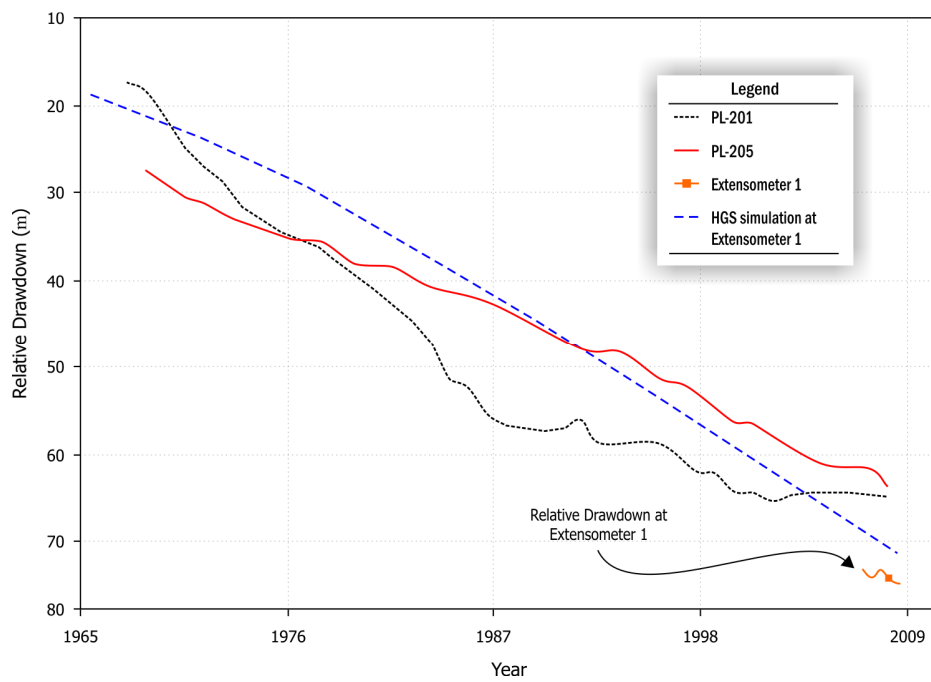


**Figure 11.** Measured and simulated relative drawdown at Extensometer 1 contrasted with measured relative drawdown of nearby long-term monitoring wells PL-201 and PL-205 (see Figs. 10 or 14 for locations, modified from Calderhead et al. (2011)).

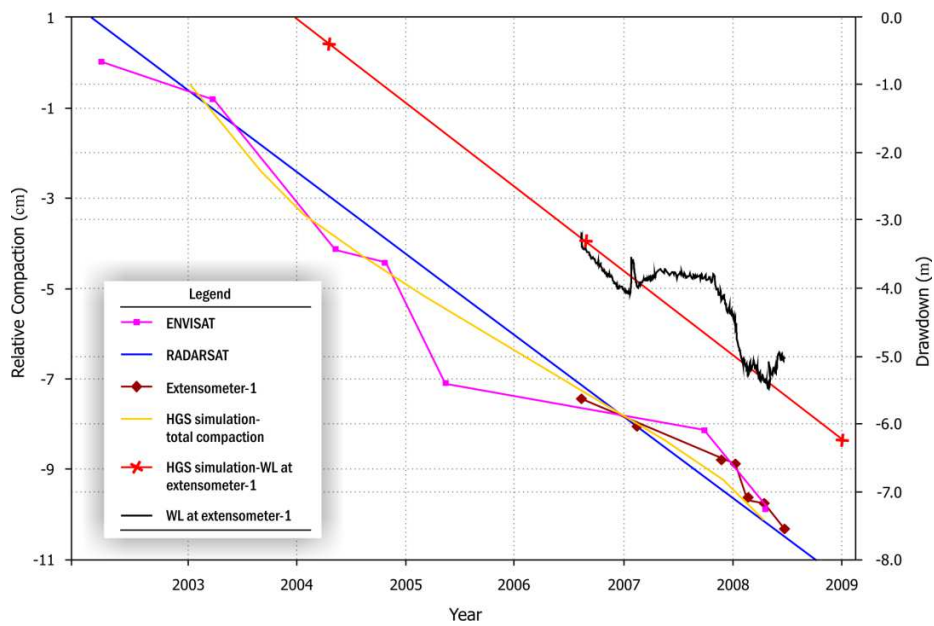


**Figure 12.** Simulated and measured total compaction at Extensometer-1 by ENVISAT ASAR, RADARSAT-1, Extensometer-1, and HGS simulation. Simulated and measured drawdown (WL) at Extensometer-1 are also included (modified from Calderhead et al. (2011)).

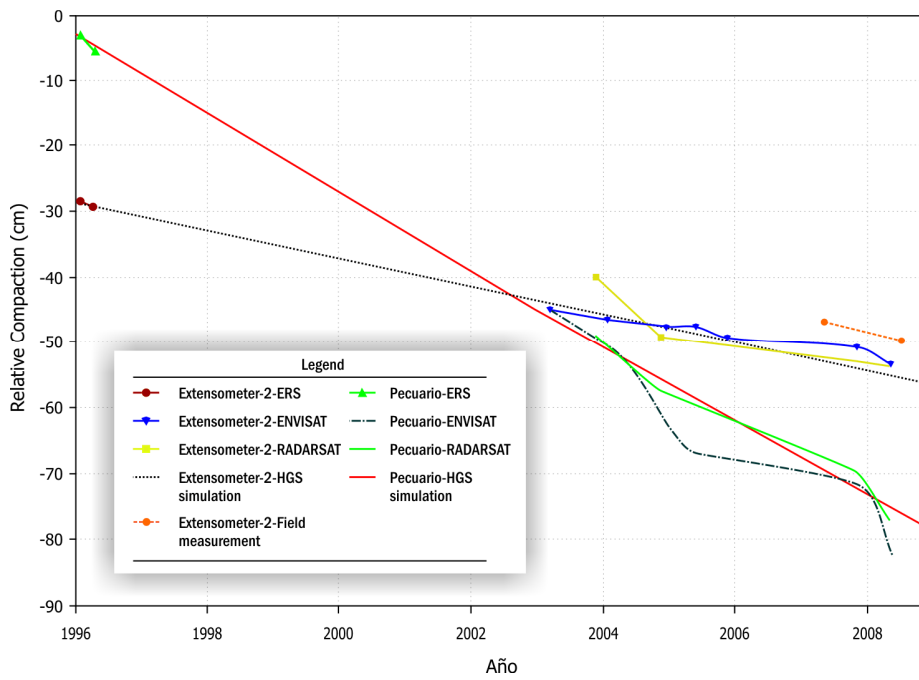


**Figure 13.** Relative compaction as a function of time at Extensometer-2 and the Pecuario well location. Simulations Compaction values are from InSAR with ENVISAT ASAR, RADARSAT-1, ERS-1, and simulated by HGS. Additionally, compaction observed with Extensometer-2 is also shown (modified from Calderhead et al. (2011)).

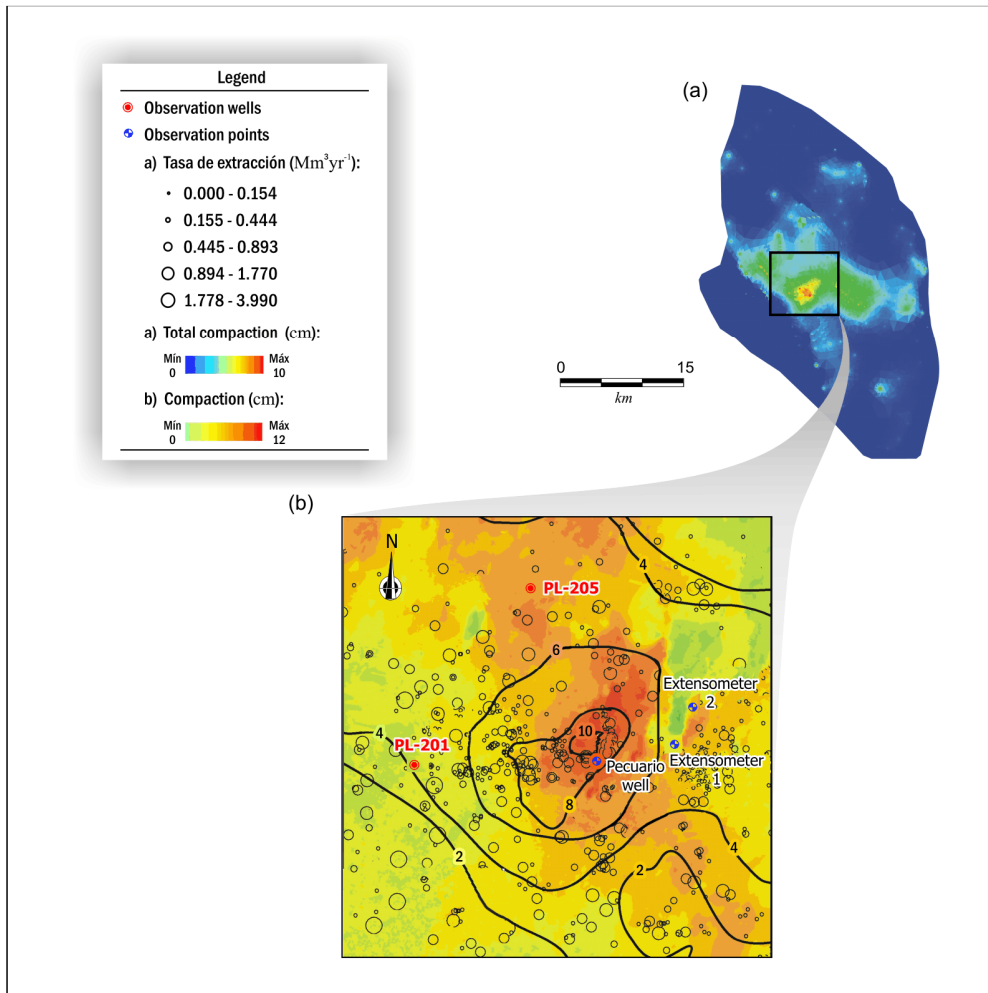


**Figure 14.** (a) HGS simulation results for the entire valley from December 5<sup>th</sup>, 2007 to May 28<sup>th</sup>, 2008; (b) HGS simulation (solid black lines) superimposed on D-InSAR subsidence map (color infilling) for the same time period (175 days). Locations of pumping wells with pumping rates are also indicated. Labels for the lines are compaction in cm ((modified from Carderhead et al. 2011)).

period.

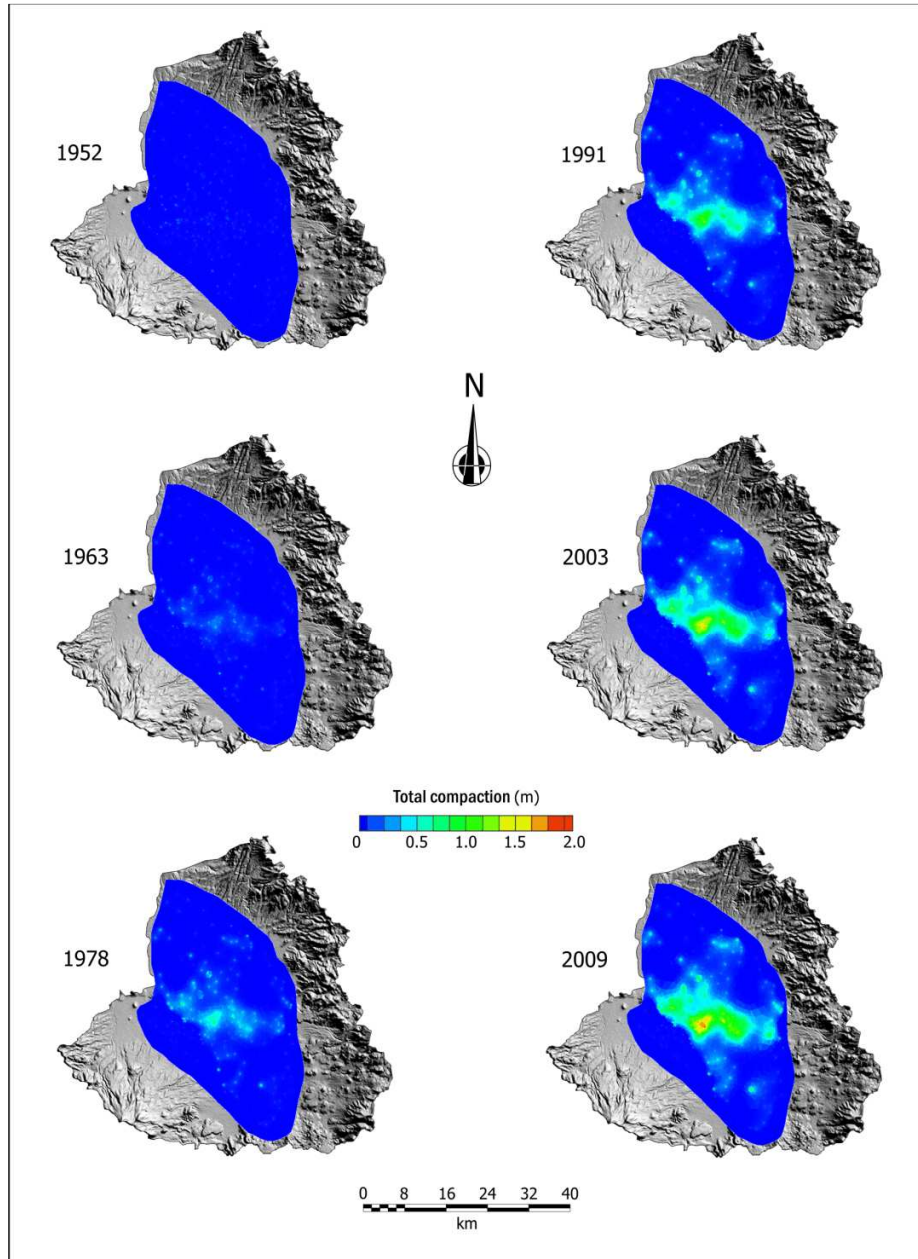


**Figure 15.** Evolution of regional land subsidence in the Toluca Valley aquifer system from 1960 to 2009 simulated with HGS (modified from Calderhead et al. (2011)).

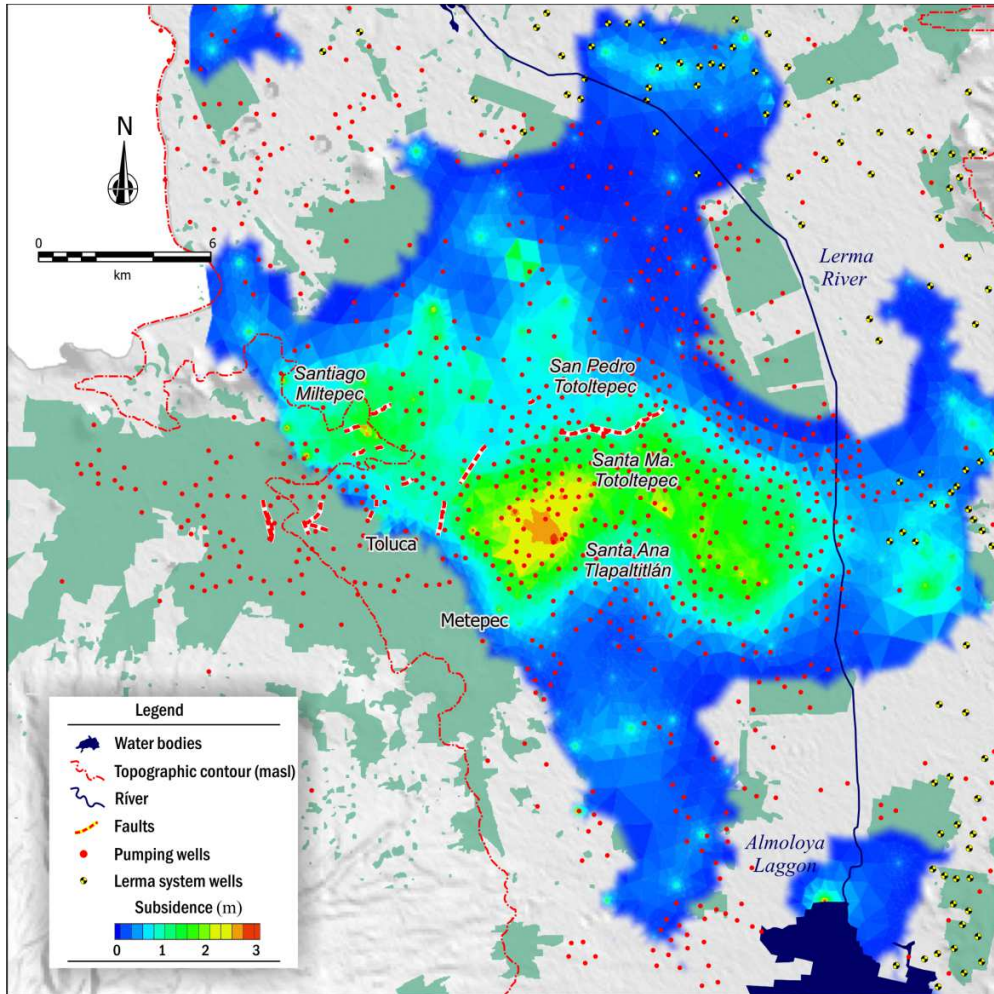


**Figure 16.** Simulated regional land subsidence in the Toluca Valley aquifer system for 2009 obtained with HGS. Also shown is the location of the pumping wells, including the Lerma system wells pumping water to the Mexico Basin, as well as the spatial distribution of faults and the urban area for 2015 delineated using Landsat images (see Fig. 15 for evolution of regional land subsidence from 1960 to 2009).